FACTOR GRAPH BASED LINEAR MINIMUM MEAN SQUARE ERROR EQUALIZATION FOR WIRELESS COMMUNICATIONS

A THESIS SUBMITTED TO
THE GRADUATE SCHOOL OF NATURAL AND APPLIED SCIENCES
OF
MIDDLE EAST TECHNICAL UNIVERSITY

BY

PINAR ŞEN

IN PARTIAL FULFILLMENT OF THE REQUIREMENTS
FOR
THE DEGREE OF MASTER OF SCIENCE
IN
ELECTRICAL AND ELECTRONICS ENG.

JULY 2014

Approval of the thesis:

FACTOR GRAPH BASED LINEAR MINIMUM MEAN SQUARE ERROR EQUALIZATION FOR WIRELESS COMMUNICATIONS

submitted by **PINAR ŞEN** in partial fulfillment of the requirements for the degree of **Master of Science in Electrical and Electronics Eng. Department, Middle East Technical University** by,

Prof. Dr. Canan Özgen
Dean, Graduate School of **Natural and Applied Sciences** _____

Prof. Dr. Gönül Turhan Sayan
Head of Department, **Electrical and Electronics Eng.** _____

Assoc. Prof. Dr. Ali Özgür Yılmaz
Supervisor, **Electrical and Electronics Eng. Dept., METU** _____

Examining Committee Members:

Prof. Dr.Yalçın Tanık
Electrical and Electronics Engineering Dept., METU _____

Assoc. Prof. Dr. Ali Özgür Yılmaz
Electrical and Electronics Engineering Dept., METU _____

Assoc. Prof. Dr. Melek Diker Yücel
Electrical and Electronics Engineering Dept., METU _____

Assoc. Prof. Dr. Çağatay Candan
Electrical and Electronics Engineering Dept., METU _____

Assoc. Prof. Dr. Emre Aktaş
Electrical and Electronics Engineering Dept., Hacettepe University _____

Date: 16.07.2014

I hereby declare that all information in this document has been obtained and presented in accordance with academic rules and ethical conduct. I also declare that, as required by these rules and conduct, I have fully cited and referenced all material and results that are not original to this work.

Name, Last Name: PINAR ŞEN

Signature :

ABSTRACT

FACTOR GRAPH BASED LINEAR MINIMUM MEAN SQUARE ERROR EQUALIZATION FOR WIRELESS COMMUNICATIONS

Pınar Şen,
M.S., Department of Electrical and Electronics Eng.
Supervisor : Assoc. Prof. Dr. Ali Özgür Yılmaz

July 2014, 76 pages

In this work, we have studied on a reduced complexity factor graph based linear minimum mean square error (LMMSE) filter as an equalizer for different wireless communication problems. First, we introduce an efficient way of computing extrinsic bit log-likelihood ratio (LLR) values for the LMMSE estimation through the previously presented graph structure in the literature compatible with higher order alphabets. In addition, we propose to adapt this graph structure so that it has the ability of including the non-white statistics of a random process. Our new structure, which corresponds to block LMMSE filtering under a Gaussian autoregressive (AR) process, has the advantage of complexity linearly increasing with the block length and the ease of incorporating the *a priori* information of the input signals whenever possible. Extensive simulations and comparisons to the theoretical calculations show that our method performs identical with the optimal block LMMSE filtering for Gaussian input signals.

Moreover, the proposed method can be used for any random process with a known

(or estimated) autocorrelation function by use of an approximation to an AR process as detailed in this study. To support this idea, we present an application for which the proposed graph structure can be used as an equalizer through the mentioned approximation. Both the intersymbol interference (ISI) and the effect of non-white noise inherent in Faster-than-Nyquist (FTN) signaling are shown to be handled by our method. In order to incorporate the statistics of noise signal into the factor graph over which the LMMSE algorithm is implemented, we suggest using a known method in the literature for modelling the noise signal as an autoregressive (AR) process. Based on these improvements, we show that the proposed low complexity receiver structure performs close to the optimal decoder operating in ISI-free ideal scenario without FTN signaling through simulations.

In the last part of our work, we propose to enlarge the state space model of the previous graph structure in order to remove inter-symbol and inter-stream interference in multiple input multiple output (MIMO) communication. The resultant representation inflicted on the graph provides a time domain equalizer having computational complexity linearly increasing with block length. Also, owing to the Gaussian assumption used in the presented cycle free factor graph, the complexity of the suggested method is not affected by the size of the signalling space. The extrinsic bit LLR transition algorithm that we introduce can be applied for this scenario straightforwardly. Overall, we provide an efficient receiver structure reaching high data rates in frequency selective MIMO systems whose performance is shown to be very close to a genie-aided matched filter bound through extensive simulations.

Keywords: linear LMMSE equalization, factor graph, Gaussian assumption, Gaussian message passing, turbo decoding, extrinsic LLR computation, colored noise, AR-process modelling, FTN-signaling, MIMO ISI channel.

ÖZ

KABLOSUZ İLETİŞİM İÇİN ÇARPAN ÇİZGE TEMELLİ DOĞRUSAL ENKÜÇÜK ORTALAMA KARESEL HATA DENKLEŞTİRİCİLER

Pınar Şen,
Yüksek Lisans, Elektrik ve Elektronik Mühendisliği Bölümü
Tez Yöneticisi : Doç. Dr. Ali Özgür Yılmaz

Temmuz 2014, 76 sayfa

Bu çalışmada, kablosuz iletişimdeki problemler için bir denkleştirici yapısı olarak kullanılabilecek düşük karmaşıklığa sahip, çarpan çizge temelli doğrusal enküçük ortalama karesel hata (LMMSE) filtresi üzerine çalıştık. Öncelikle, literatürde önceden önerilmiş olan çizge temelli LMMSE kestirimi için, daha yüksek dereceli kipleme alfabeleri ile uyumlu ve verimli bir dışsal ikil (bit) log-olabilirlik oranı (LLR) hesaplama yöntemi geliştirdik. Ayrıca, bu çizge yapısını, bir rastsal sürecin beyaz olmayan istatistiklerini de bünyesine dahil edebilecek şekilde uyarladık. Gauss özbağlanımlı (AR) bir süreç için blok LMMSE filtrelemeye karşılık gelen yeni yapımız, blok uzunluğu ile doğrusal olarak artan karmaşıklığa ve girdi sinyalleri hakkında bilinen önsel (*a priori*) bilgiyi dahil etme kolaylığına sahiptir. Kapsamlı benzetim sonuçları ve teorik değerler ile yapılan kıyaslamalar, metodumuzun Gauss girdiler için eniyi blok LMMSE filtre ile birebir aynı çalıştığını göstermektedir.

Ayrıca, önerilen yöntem bilinen (ya da kestirilen) bir özilinti fonksiyonu olan herhangi bir rastsal süreç için, detayları bu çalışmada anlatıldığı gibi bir AR sürece yak-

laştırım yardımı ile kullanılabilir. Bu fikri desteklemek için, önerilen çizge yapısının bahsedilen yaklaştırım üzerinden bir denkleştirici olarak kullanıldığı bir uygulama sunulmaktadır. Nyquist'ten daha hızlı (FTN) sinyalizasyonun doğasında varolan hem semboller arası girişim (ISI), hem de beyaz olmayan gürültü etkilerinin yöntemimiz tarafından ele alındığı gösterilmektedir. Gürültü sinyalinin istatistiklerini, LMMSE algoritmasının üzerinde gerçekleştirildiği çarpan çizgeye dahil etmek amacıyla, gürültü sinyalini AR süreç ile modellemek için literatürde bilinen bir yöntemi kullanmayı öneriyoruz. Bu iyileştirmelere dayanarak, önerdiğimiz düşük karmaşıklıktaki alıcı yapısının FTN sinyalizasyonun yapılmadığı ISI'sız senaryodaki eniyi kodçözücüye yakın çalıştığı benzetimler üzerinden gösterilmektedir.

Çalışmamızın son kısmında, çoklu girdi çoklu çıktı (MIMO) haberleşmesinde semboller arası ve sinyal akışları arası girişimi kaldırmak amacıyla, eski çizge yapısının durum uzay modelini genişletmeyi öneriyoruz. Sonuçta çizgeye yansıtılan gösterim, zamanda blok uzunluğu ile doğrusal artan karmaşıklıkta bir denkleştirici sağlamaktadır. Ayrıca, sunulan döngüsüz çarpan çizgede kullanılan Gauss varsayımı sayesinde, önerilen yöntemin karmaşıklığı sinyal uzayının boyutundan etkilenmez. Geliştirdiğimiz dışsal bit LLR hesaplama yöntemi bu senaryoya doğrudan uygulanabilir. Bütüncül olarak, frekans seçiciliğine sahip MIMO sistemlerde yüksek bilgi hızlarına ulaşan ve başarımının cin destekli uyumlu süzgeç sınırına çok yakın çalıştığı benzetimlerce gösterilen verimli bir alıcı yapısı öneriyoruz.

Anahtar Kelimeler: Doğrusal LMMSE denkleştiricisi, çarpan çizge, Gauss varsayımı, Gauss mesaj iletimi, turbo çözümleme, dışsal LLR hesaplaması, renkli gürültü, AR süreç modellemesi, FTN-sinyalleme, MIMO ISI kanal.

To my family, my sister and my best friend

ACKNOWLEDGMENTS

First, I would like to thank my supervisor, Ali Özgür Yılmaz, for his continuous support and mentorship which guide me in both academic and personal life. It is a great pleasure to work in new and exciting concepts in communications with such a successful and modest advisor for me. I am also grateful for relaxing conversations which we have with him and his wife, Bahar. They influenced my philosophy of life.

The valuable instructors in our department, particularly the ones teaching in Telecommunication field who helped me expand my vision have a special place for me. The precious time that I spent during my Master studies in Telecommunication group contributed a lot to my academic life.

I am indebted to my first friends in Telecommunication Laboratory for helping me get used to academic environment. Special thanks to Gökhan Muzaffer Güvensen and Erman Köken for their invaluable friendship and motivating chat in my hard times. I will remember our beautiful memories in the lab with Seçil Özdemir, Neyre Tekbıyık, Fatih Özçelik, Samet Gelincik and Oktay Koç. Our group have later become more enjoyable with Ali Bulut Üçüncü and Alptekin Yılmaz with our pleasant talk. As two of my dearest friends, I will miss the smiling face of Mürsel Karadaş and the endless energy of Selim Özgen. They teach me to be open to differentness. Moreover, I thank all of my friends who are not mentioned here for all their contributions to my personality and my life.

It is a pleasure for me to be financially supported by The Scientific and Technological Research Council of Turkey (TÜBİTAK) during my Master studies covering two years. In addition, thanks to the research project supported by Aselsan A.Ş., I had a chance to work with Ali Özgür Yılmaz and to focus on the core subject of our study which is developed and presented here.

I thank my family for being so supportive and caring parents. It is priceless to know

that they always stand behind me and my sister with their unconditional love. From the beginning of our education life, they have always taken close interest in our success. My devoted mother and my father, who made us love mathematics as our first teacher at home, have a great place in my achievements. Separately, special thanks go to my sister Cansu, who has a very special place in my life. Alongside of our invaluable memories since our childhood, I am grateful for her relaxing and cheerful personality which has a healing effect on me in my hard times. Although Cansu is my little, cute and precious sister, she is an older sister to me when I need. Lastly, I am obliged to another special person, my boy friend, Tuğcan Aktaş who is literally always near me under all types of difficulties in both academic and personal life. It is a great pleasure to work with such a giving and encouraging colleague who guided me and kept me in countenance believingly most of the times throughout my studies. I feel so lucky to have him as my best and irreplaceable friend and also my best research partner in our lab.

TABLE OF CONTENTS

LIST OF TABLES

TABLES

LIST OF FIGURES

FIGURES

LIST OF ABBREVIATIONS

APP	A Posteriori Probability
AR	Auto-regressive
AWGN	Additive White Gaussian Noise
BER	Bit-Error-Ratio
BPSK	Binary Phase Shift Keying
BCJR	Bahl-Cocke-Jelinek-Raviv
FDE	Frequency Domain Equalization
FFT	Fast Fourier Transform
FTN	Faster Than Nyquist
GMP	Gaussian Message Passing
ISI	Inter-Symbol Interference
JG	Joint Gaussian
LMMSE	Linear Minimum Mean Square Error
LLR	Log-likelihood Ratio
MFB	Matched Filter Bound
MIMO	Multiple Input Multiple Output
MSE	Mean Square Error
OFDM	Orthogonal Frequency Division Multiplexing
pdf	Probability Density Function
PSD	Power Spectral Density
PSK	Phase Shift Keying
QAM	Quadrature Amplitude Modulation
rRC	Root-Raised-Cosine
SC-FDE	Single Carrier Frequency Domain Equalization
SISO	Single Input Single Output
SNR	Signal-to-Noise Ratio
ZMCSCG	Zero Mean Circularly Symmetric Complex Gaussian

CHAPTER 1

INTRODUCTION

Together with the development of factor graphs and Gaussian message passing (GMP) rules on linear state space models, filtering operations have lately been implemented with limited computational complexity and memory requirements [27, 28]. One example is LMMSE filtering, which is in fact equivalent to performing two-way Kalman filtering operations through a factor graph under a Gaussian assumption [27]. A recently studied version of LMMSE filtering was implemented on a factor graph under additive white Gaussian noise in [17, 29], which has a complexity linearly increasing with block length of the input signal; whereas the computational complexity of the conventional block LMMSE filtering is increasing approximately with the cube of the block length [41]. Another advantage comes along from the Gaussian assumption. Since the LMMSE filter operates on the input signal with the assumption that it is coming from a Gaussian alphabet [29], its complexity is independent from the discrete alphabet size utilized in communication applications.

We base our study on the state space graph structure presented in [17, 29] and improve it for some communication problems. One important contribution of our study is the proposed LLR exhange algorithm for M-QAM signaling. LMMSE equalizers involved in turbo decoders need a method for transition to binary domain, i.e., to bit LLR domain. In the literature, there were effective approaches to obtain bit LLRs from the LMMSE equalizer outputs, such as the Wang-Poor approach [40, 42] and the Joint Gaussian (JG) approach [25]. However, applying the Wang-Poor or JG approaches directly is computationally intensive for factor graphs. Although a simplified expression for extrinsic LLR computation was obtained in [17] for BPSK

signaling, there is no such work for higher order constellations in the literature within our knowledge. To fill up this gap, we derive a transformation from the graph outputs to the bit LLRs by using the Wang-Poor approach for higher order modulation alphabets. Owing to this key connection, extrinsic bit LLR values can be obtained in accordance with the graph solution without any major complexity increase.

Among the communication problems, we focused on implementing LMMSE filtering with reduced complexity under non-white noise processes. The factor graph approach to LMMSE filtering under white Gaussian noise in [17] provides a practical receiver structure particularly for ISI channel, which is frequently encountered in wireless communications. However, there are other problems in the literature in which the statistics of non-white noise processes are needed to be taken into consideration. For example, in Faster-than-Nyquist (FTN) signaling method [32] and channel shortening for long, sparse ISI channels [34], the inherent non-white noise processes are handled by various solutions including whitening filters. In addition, colored noise processes also appear in radar [5] and speech enhancement problems [15].

Although forward Kalman filtering matrix operations are adapted for Gaussian AR noise processes in [15], there is no reduced complexity work on factor graphs which includes the effect of the colored noise in the literature to the best of our knowledge. Hence, what we propose is a factor graph based LMMSE filtering approach which implements two-way Kalman filtering operations with the ability of including the statistics of the non-white Gaussian noise. We basically extend the state variables on the factor graph of [17] by joining them with the variables of the noise process as introduced in [15]. The proposed method, which can be generalized to other noise statistics through an approximation is first studied under the Gaussian AR process framework. Through extensive simulations, it is shown that the proposed technique, which has the advantage of reduced computational complexity and less requirement of memory, performs identical with the optimal block LMMSE filtering solution for Gaussian input signals. Theoretical derivations also confirmed our simulation results. Another benefit of the proposed method comes from its factor graph based structure in which the existing *a priori* information of the input signals can be effortlessly incorporated as needed in many iterative communication receivers. Hence, it can be a practical way of block LMMSE filtering for the mentioned problems with non-

white noise processes. On the other hand, we compare its performance results to the LMMSE equalizer operating under white process assumption and look for the asymptotic behaviour of those two LMMSE filters. Although for high noise correlation there is a remarkable performance gain that our method provides, asymptotically (for high signal to noise ratio (SNR) values) they exhibit very similar results. In addition, the performance gain of our method also reduces as the correlation of the noise process decreases. Hence, it depends on the specific characteristics of the problem at hand.

As an example, we have studied on a communication application, FTN signalling, in which we handle the inherent ISI effect and the colored noise by our proposed graph based LMMSE filtering method. FTN signaling is one of the proposed techniques to increase the spectral efficiency in the literature. The first studies on FTN signaling concept date back to 1970s [30]. But it has received much more attraction recently as a means of providing higher transmission rate beyond the Nyquist criterion in the same spectral shape consuming the same energy per bit [1]. By contrast to the classical scenario using T-orthogonal pulse shape, the pulses in FTN signaling can be packed by violating the Nyquist rate without decreasing the minimum Euclidean distance (d^2_{min}) in the signaling space [37]. (The minimum symbol time for which d^2_{min} is not below the value of the case with orthogonal pulse shape is called the Mazo limit [36]).

Since FTN signaling has more symbols to be packed in the time interval T than the conventional orthogonal signaling, there exists intentional ISI which causes an increase in the receiver complexity. However, thanks to the recent studies on practical receivers, it is still possible to achieve the same error rate performance as the conventional way. Among the latest ones, a reduced trellis based algorithm ($\mathcal{M}$-BCJR) having a linearly increasing complexity with block length is proposed in [32]. But its complexity increases exponentially with constellation size and the number of ISI taps due to the necessity of high $\mathcal{M}$ value. Moreover, $\mathcal{M}$-BCJR needs an optimized whitening filter for each channel realization at the receiver side so as to enjoy a good performance as mentioned in [32], which makes this method hard to implement in real time for fading environments. In another work [39], frequency domain equalization with an additional complexity of fast Fourier transform (FFT) and inverse-FFT operations is analysed for uncoded FTN schemes. It brings a performance loss because of

the lack of coding and turbo operation and also a decrease in efficiency due to use of cyclic prefix. On the other hand, we propose to use a low complexity (linearly increasing with block length) and practical reduced LMMSE equalization method to remedy the ISI effect due to FTN signaling. Furthermore, our receiver structure is perfectly suited for high constellation sizes, since the number of the elements in the alphabet is irrelevant to our equalization process. In a more detailed way, we develop a factor graph-based LMMSE algorithm in which the non-white noise inherent in FTN is taken into consideration. Although the receiver structure that we propose is shown to perform very close to the optimal decoder operating under non-ISI, i.e., additive white Gaussian noise (AWGN) channel through extensive simulations for lower packing ratio, we have observed that equalization performance of LMMSE filtering gets worse while increasing transmission rate due to sub-optimality caused by the Gaussian assumption. We have also compared our results with the performance of [17] under white noise assumption and observed that there is a trade off with whether the non-white statistics of noise process should be taken into consideration or not depending on the correlation characteristics.

In the final part of our study, we consider frequency selective MIMO systems. MIMO systems have attracted much attention in recent years since they potentially provide high spectral efficiency in wireless communication applications. Yet, they require complicated receiver structures so as to handle the distortion caused by the wireless channel characteristics such as ISI resulting from the frequency selectivity of the channel between each transmit and receive antenna pair.

In recent studies, low complexity methods are proposed to mitigate those distorting effects in MIMO ISI channels. Orthogonal frequency division multiplexing (OFDM) based methods hold an important place in the literature, but OFDM is confirmed to have some serious drawbacks including peak to average power ratio problem, high sensitivity to carrier frequency offset and diversity loss without channel coding [18, 31], which calls for another popular technique, single carrier frequency domain equalization (SC-FDE). SC-FDE has been a highly attractive approach over the last years since it does not include the disadvantages in multi carrier modulation and still enjoys low complexity, which is mainly due to the use of FFT and inverse FFT [13,18,31,43]. However, FDE is a method which is devised under the assumption

of quasi static Rayleigh fading, i.e., the channel does not change during the transmission of one block and changes independently from one block to another. Although this is a valid assumption for slowly varying channels, the performance of classical FDE is degraded under fast fading with large Doppler spread since the channel matrix in frequency domain is no longer diagonal. Dividing the transmission block into smaller sub-blocks where the channel taps remain constant will not be an effective solution either since efficiency would drop due to a larger percentage of the cyclic prefix.

As an alternative, low complexity time domain approaches have drawn interest once more for frequency selective MIMO systems in fading environments from the perspective of the lately studied factor graph theory [11, 24, 26–29]. Belief propagation and sum product algorithms on factor graphs were proposed for both single input single output (SISO) and MIMO systems [10, 23], but they have $O(M^{\tilde{P}})$ complexity per symbol where M is the constellation size and $\tilde{P}$ is the total number of *non-zero* interferers. Hence, the Gaussian assumption which provides constant complexity with increasing alphabet size has become popular. As an example, Kalman filtering was proposed for coded frequency selective MIMO systems in [35]. However, it has $O(P^3)$ complexity per symbol where P is the number of interferers, and more importantly lacks the improvement that backward recursion provides. On the other hand, the GMP rules including Kalman filtering (forward recursion) and Kalman smoothing (backward recursion) operations are derived [24, 29] and used in the implementation of LMMSE equalization on factor graphs. As we mention, this approach has the advantage of low complexity linearly increasing with block length N as compared to conventional block LMMSE filter's $O(N^3)$ complexity [41]. Although factor graph structures with cycles using the GMP rules were proposed for SISO and MIMO ISI channels respectively in [9, 19], our main focus is the cycle free ones due to exact equivalence to LMMSE filtering avoiding any iterations. There are two different cycle free factor graph structures presented in the literature for SISO systems [11, 17]. The generalization of [11] to MIMO ISI channels was proposed in [12], which still has $O(P^3)$ complexity per symbol. In addition, the mentioned studies including the GMP rules do not have any performance results for modulation types other than BPSK sig-

naling due to the lack of LLR exchange algorithm.

In our study, however, we reduce the complexity to $O(P^2)$ per symbol with the help of a factor graph structure which takes its roots from [17]. In our extension for MIMO ISI systems, there are two main mechanisms which provide the decrease in complexity:

- Using Matrix inversion lemma while computing the GMP rules,
- The block-wise shifting structure of the proposed graph that allows computationally intensive steps to be conducted sporadically.

Moreover, using Gaussian approximation of GMP rules keeps the complexity of the graph algorithm constant with the increasing constellation size. In addition, the presented approach here brings the ease of involving existing *a priori* information of the transmitted symbols, hence perfectly matched with the turbo concept for coded systems. It is also well suited to fast fading environments since the channel taps (possibly time-varying) are directly included in the graph. Therefore, the proposed structure is a very advantageous way of implementing LMMSE filtering for equalization of MIMO ISI channels. Consequently, we present a state space graph for time domain LMMSE equalization of MIMO ISI channels with a reduced complexity as compared to the techniques in the literature. Overall, the performance of the proposed structure is shown to be very close to a hypothetical genie-aided matched filter bound [4] through extensive simulations, which makes it an efficient receiver that can reach high data rates in frequency selective MIMO systems.

In summary, we deal with the graph based LMMSE equalization for various problems in communication systems. In Chapter 2, we give the principles of the previously proposed graph structure in [17] for LMMSE equalization of SISO ISI channels under white Gaussian noise processes for BPSK signalling and we present a method for using LMMSE equalization with higher order constellations. In Chapter 3, we improve the graph structure mentioned in Chapter 2 so that it has the ability to include the non-white statistics of a Gaussian AR process. In addition, an approximation tech-

nique for any stationary random process to Gaussian AR process in the literature is described. Chapter 4 demonstrates an application, in which the inherently involved colored process and ISI effect are handled by the proposed graph structure in Chapter 3, through the mentioned approximation. The generalization of the graph structure and the algorithm explained in Chapter 2 to frequency selective MIMO systems are detailed in Chapter 5. Over the whole study, we present the performance results of our proposed methods through extensive simulations as compared to other alternatives and we discuss the advantage and disadvantages. Finally, Chapter 6 concludes our work.

The notations used are organized as follows. Lower case letters (e.g., x) denote scalars, lower case bold letters (e.g., $\mathbf{x}$) denote vectors, upper case bold letters (e.g., $\mathbf{X}$) denote matrices. For a given random variable x; m_x, v_x, w_x and $w_x m_x$ denote its mean, variance, weight and weighted mean values respectively where $w_x \triangleq v_x^{-1}$. For a given vector random variable $\mathbf{x}$; $\mathbf{R_x}, \mathbf{m_x}, \mathbf{V_x}, \mathbf{W_x}$ and $\mathbf{W_x m_x}$ denote its autocorrelation matrix, mean vector, covariance matrix, weight matrix and weighted mean vector respectively where $\mathbf{W_x} \triangleq \mathbf{V_x}^{-1}$. The indicators $()^*$, $()^H$, and $E\{\}$ denote conjugate, Hermitian transpose and expectation operations respectively and $\mathbf{I}$ denotes the identity matrix of proper size. The operation $diag\{\mathbf{A}\}$ is defined as the diagonal elements of a matrix $\mathbf{A}$.

CHAPTER 2

FACTOR GRAPH BASED LMMSE FILTERING FOR SISO ISI CHANNELS UNDER WHITE GAUSSIAN NOISE

In this chapter, we present a state space based reduced complexity factor graph used for LMMSE filtering of SISO systems suffering from multipath effects of wireless channels under additive white Gaussian noise. After describing the system model, we present the details of the graph structure and message passing rules under a Gaussian approximation. To make a transition between the LMMSE estimator operating in the Gaussian domain and the LLR estimator operating in binary domain for coded systems, we provide an extrinsic LLR exchange algorithm in a generalized form that is applicable to higher order modulation alphabets. Finally, we present the performance results of the LMMSE equalizer with the proposed LLR exchange algorithm through simulations.

2.1 System Model

We consider a baseband single carrier SISO communication system using complex valued constellations M-PSK or M-QAM in our setting. Fig. 2.1 presents the whole block diagram of the transmitter and the receiver structures. At the transmitter side, after the coded information bits are interleaved and modulated, the resultant symbols are sent over the ISI channel. At the receiver side, an iterative receiver structure including the factor graph based LMMSE equalizer and an *a posteriori* probability (APP) decoder is operated. After a predetermined number of iterations, bit decisions are obtained.

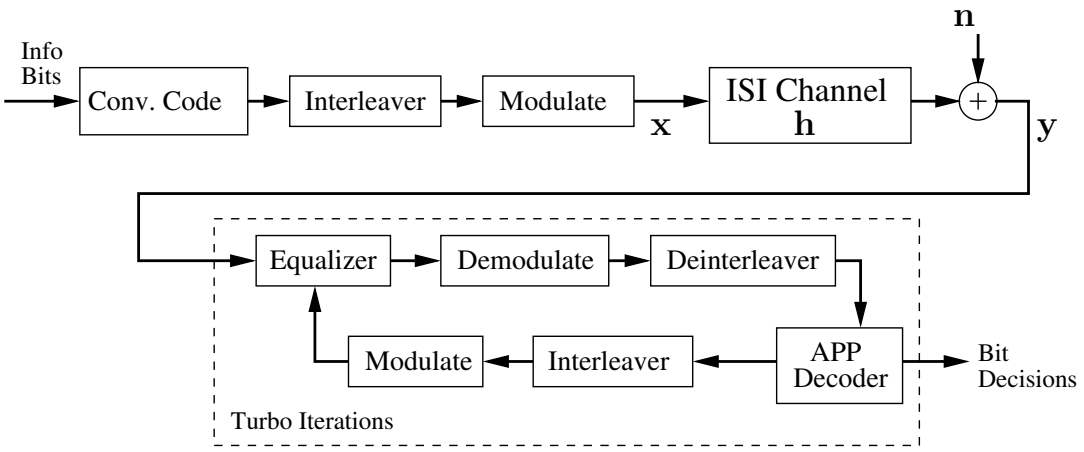

Figure 2.1: Sytem model for SISO ISI systems

We can model the discrete-time received signal at time k as

$$y_k = \sum_{i=0}^{L-1} h_i x_{k-i} + n_k\,; \quad k = 1, 2, \ldots, N + L - 1, \tag{2.1}$$

where L is the number of channel taps; N is the transmission block length; h_i is the channel coefficient at time i; x_k and y_k are the transmitted symbol and received observation at time k respectively; and n_k represents additive white zero mean circularly symmetric complex Gaussian (ZMCSCG) noise with variance N_0 at time k, i.e., $n_k \sim CN(0, N_0)$. The average symbol energy E_s is defined as $E\{|x_k|^2\} \triangleq E_s$ and channel memory J is defined as $J \triangleq L - 1$.

2.2 LMMSE Filtering Based on Reduced Complexity Factor Graph

Conventional block LMMSE filtering has a complexity increasing with the cube of the transmission block length N, i.e., $O(N^3)$ [41]. However, in [17], it is shown that LMMSE filtering can be implemented on a factor graph which has a complexity increasing linearly with N. In the following subsections, we will give the details of the proposed graph in [17, 27] on which we base our study. In addition, we will provide a generalized LLR exchange algorithm which is compatible with the higher order modulation alphabets.

2.2.1 State Space Representation

For the system described in Fig. 2.1, the observation vector at time k given in (2.1) can be rewritten as

$$y_k = \overline{\mathbf{h}}\, \overline{\mathbf{x}}_k + n_k \; ; \quad k = 1, 2, \ldots, N + J \tag{2.2}$$

where $\overline{\mathbf{h}}$ denotes the channel coefficient vector of length L and $\overline{\mathbf{x}}_k$ denotes the state variable vector at time k which is composed of the input variables between time $k - L + 1$ and k as given by

$$\overline{\mathbf{h}} = [h_J \quad h_{J-1} \quad \ldots \quad h_0], \quad \text{and} \tag{2.3}$$

$$\overline{\mathbf{x}}_k = [x_{k-J} \quad x_{k-J+1} \quad \ldots \quad x_k]^T_{L\times 1}. \tag{2.4}$$

(2.2)-(2.4) are used to construct the state space graph representation of the SISO ISI channels [17, 27]. As shown in Fig. 2.2, (2.2)-(2.4) are used to reach the observation at time k in the k^{th} building block. Since the overall graph structure is composed of consecutive building blocks, state variable vector $\overline{\mathbf{x}}_k$ needs to be shifted as going to the next time instant. For advancing to the next time instant, $k+1$, transition matrices are defined as

$$\mathbf{G} = \begin{bmatrix} \mathbf{0}_J & \mathbf{I}_J \\ 0 & \mathbf{0}_J^T \end{bmatrix}_{L\times L}, \mathbf{f} = \begin{bmatrix} \mathbf{0}_J \\ 1 \end{bmatrix}_{L\times 1}, \tag{2.5}$$

where $\mathbf{0}_J$ denotes the all zero vector of length J, and $\mathbf{I}_J$ denotes the identity matrix of size $J \times J$. It can be seen that the state variable vector $\overline{\mathbf{x}}_{k+1}$ at time $k + 1$ is reached through the use of $\mathbf{G}$ and $\mathbf{f}$ as follows

$$\overline{\mathbf{x}}_{k+1} = \mathbf{f}\; x_{k+1} + \mathbf{z}_{k+1}, \quad \text{where} \tag{2.6}$$

$$\mathbf{z}_{k+1} = \mathbf{G}\; \overline{\mathbf{x}}_k \tag{2.7}$$

$$= \begin{bmatrix} x_{k-J+1} \\ x_{k-J+2} \\ \vdots \\ x_k \\ 0 \end{bmatrix}.$$

The factor graph representation corresponding to (2.2)-(2.7) can be inspected in Fig. 2.2. LMMSE equalization is performed on this cycle free graph with the help of the Gaussian Message Passing (GMP) rules which is detailed in the next subsection.

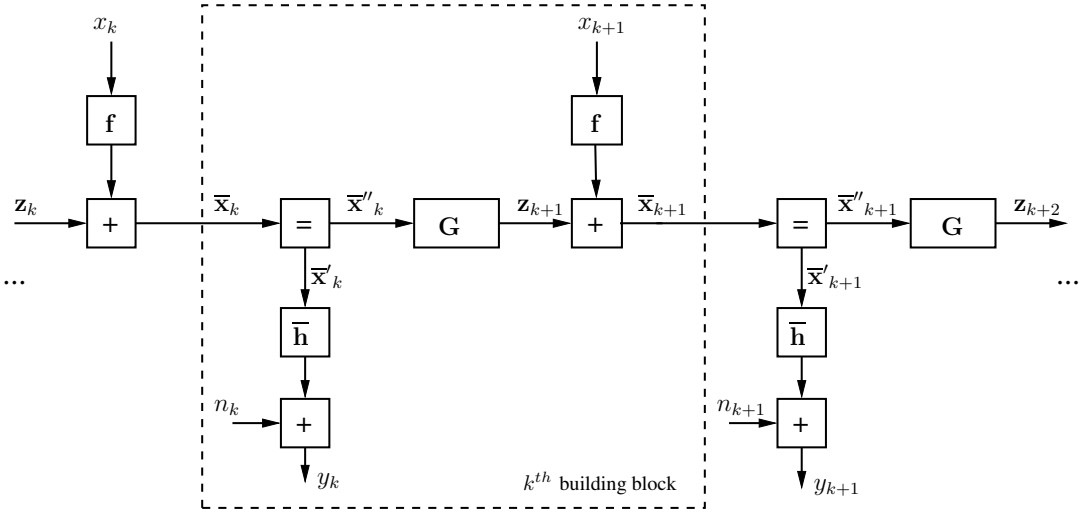

Figure 2.2: Factor Graph Structure of LMMSE Filtering for SISO ISI systems

2.2.2 Gaussian Message Passing (GMP) Rules

In the graph structure given in Fig. 2.2, each scalar state variable or state vector is assumed to have a Gaussian distribution. This assumption provides ease of computation for message passing. In other words, scalar variables such as x_k are represented by mean m_{x_k} and variance v_{x_k} while state vectors such as $\overline{\mathbf{x}}_k$ are represented by mean vector $\mathbf{m}_{\overline{\mathbf{x}}_k}$ and covariance matrix $\mathbf{V}_{\overline{\mathbf{x}}_k}$ on the graph. The main purpose is to obtain the *a posteriori* mean $(\mathbf{m}_{\overline{\mathbf{x}}_k}^{post})$ and covariance $(\mathbf{V}_{\overline{\mathbf{x}}_k}^{post})$ of the state variables which are calculated through the GMP rules applied in forward and backward recursions. The GMP rules, which are indeed equivalent to Kalman filtering (through forward recursion) and Kalman smoothing (through backward recursion) operations corresponding to each block on the graph, are performed by using the mean and variance of the state variables [17, 24, 29]. The existing *a priori* information coming from the APP decoder is also incorporated into the graph under the Gaussian assumption by $(m_{x_k}^{\downarrow},v_{x_k}^{\downarrow})$. The transition between LLR domain and Gaussian domain will be explained in Section 2.2.3.

In Table 2.1, some of the GMP rules for basic blocks [17, 29] are provided, where the weight matrix $\mathbf{W} \triangleq \mathbf{V}^{-1}$, and arrows indicate the message directions. The main idea behind the GMP rules corresponding to each basic building block comes from the Gaussian assumption which states that all the variables in the input and output branches connected to the basic building block have Gaussian distribution. Short explanations related to each basic building block is given with a simple example below.

Table2.1: GMP Rules for Basic Building Blocks [17, 29]

Blocks	GMP Rules	
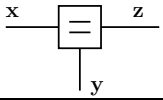	$\overrightarrow{\mathbf{W}}_{\mathbf{z}} = \overrightarrow{\mathbf{W}}_{\mathbf{x}} + \mathbf{W}_{\mathbf{y}}^{\uparrow}$ $\overrightarrow{\mathbf{W}}_{\mathbf{z}}\overrightarrow{\mathbf{m}}_{\mathbf{z}} = \overrightarrow{\mathbf{W}}_{\mathbf{x}}\overrightarrow{\mathbf{m}}_{\mathbf{x}} + \mathbf{W}_{\mathbf{y}}^{\uparrow}\mathbf{m}_{\mathbf{y}}^{\uparrow}$	(2.8) (2.9)
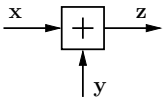	$\overrightarrow{\mathbf{V}}_{\mathbf{z}} = \overrightarrow{\mathbf{V}}_{\mathbf{x}} + \mathbf{V}_{\mathbf{y}}^{\uparrow}$ $\overleftarrow{\mathbf{V}}_{\mathbf{x}} = \overleftarrow{\mathbf{V}}_{\mathbf{z}} + \mathbf{V}_{\mathbf{y}}^{\uparrow}$ $\overrightarrow{\mathbf{m}}_{\mathbf{z}} = \overrightarrow{\mathbf{m}}_{\mathbf{x}} + \mathbf{m}_{\mathbf{y}}^{\uparrow}$ $\overleftarrow{\mathbf{m}}_{\mathbf{x}} = \overleftarrow{\mathbf{m}}_{\mathbf{z}} - \mathbf{m}_{\mathbf{y}}^{\uparrow}$	(2.10) (2.11) (2.12) (2.13)
	$\overrightarrow{\mathbf{V}}_{\mathbf{y}} = \mathbf{A}\,\overrightarrow{\mathbf{V}}_{\mathbf{x}}\,\mathbf{A}^{H}$ $\overrightarrow{\mathbf{m}}_{\mathbf{y}} = \mathbf{A}\,\overrightarrow{\mathbf{m}}_{\mathbf{x}}$	(2.14) (2.15)
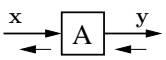	$\overleftarrow{\mathbf{W}}_{\mathbf{x}} = \mathbf{A}^{H}\,\overleftarrow{\mathbf{W}}_{\mathbf{y}}\,\mathbf{A}$ $\overleftarrow{\mathbf{W}}_{\mathbf{x}}\,\overleftarrow{\mathbf{m}}_{\mathbf{x}} = \mathbf{A}^{H}\,\overleftarrow{\mathbf{W}}_{\mathbf{y}}\,\overleftarrow{\mathbf{m}}_{\mathbf{y}}$	(2.16) (2.17)

Equality Block: When the state variable vectors $\mathbf{x}$ and $\mathbf{y}$ enter the equality block given in Fig. 2.3, their probability density functions (pdf) are multiplied to reach the scaled pdf of the output state variable vector $\mathbf{z}$ [27]. Since $\mathbf{x}$, $\mathbf{y}$ and $\mathbf{z}$ are all assumed to be Gaussian random variables here, it is easy to write the relation in terms of weight and weighted mean values of the state variables given in (2.8)-(2.9).

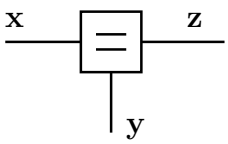

Figure 2.3: Basic Building Blocks-Equality

Example 1: Let $\mathbf{x}$ and $\mathbf{y}$ are input state vectors of length-3 with characteristics

$$\overrightarrow{\mathbf{m}}_{\mathbf{x}} = \begin{bmatrix} 1.3 \\ -0.9 \\ 1.1 \end{bmatrix}, \quad \overrightarrow{\mathbf{V}}_{\mathbf{x}} = \begin{bmatrix} 0.3 & -0.01 & 0.02 \\ -0.01 & 0.25 & 0.05 \\ 0.02 & 0.05 & 0.35 \end{bmatrix};$$

$$\overrightarrow{\mathbf{m}}_{\mathbf{y}} = \begin{bmatrix} 0.8 \\ -0.3 \\ 0.9 \end{bmatrix}, \quad \overrightarrow{\mathbf{V}}_{\mathbf{y}} = \begin{bmatrix} 0.27 & 0.07 & -0.03 \\ 0.07 & 0.4 & 0.06 \\ -0.03 & 0.06 & 0.22 \end{bmatrix}.$$

Then, the information related to output state variable vector $\mathbf{z}$ is reached by using (2.8)-(2.9) as

$$\begin{aligned} \overrightarrow{\mathbf{W}}_{\mathbf{z}} &= \begin{bmatrix} 0.3 & -0.01 & 0.02 \\ -0.01 & 0.25 & 0.05 \\ 0.02 & 0.05 & 0.35 \end{bmatrix}^{-1} + \begin{bmatrix} 0.27 & 0.07 & -0.03 \\ 0.07 & 0.4 & 0.06 \\ -0.03 & 0.06 & 0.22 \end{bmatrix}^{-1} \\ &= \begin{bmatrix} 7.3541 & -0.6377 & 0.5508 \\ -0.6377 & 6.8998 & -1.4671 \\ 0.5508 & -1.4671 & 7.8419 \end{bmatrix}, \end{aligned}$$

$$\begin{aligned} \overrightarrow{\mathbf{W}}_{\mathbf{z}}\overrightarrow{\mathbf{m}}_{\mathbf{z}} &= \begin{bmatrix} 0.3 & -0.01 & 0.02 \\ -0.01 & 0.25 & 0.05 \\ 0.02 & 0.05 & 0.35 \end{bmatrix}^{-1} \begin{bmatrix} 1.3 \\ -0.9 \\ 1.1 \end{bmatrix} + \begin{bmatrix} 0.27 & 0.07 & -0.03 \\ 0.07 & 0.4 & 0.06 \\ -0.03 & 0.06 & 0.22 \end{bmatrix}^{-1} \begin{bmatrix} 0.8 \\ -0.3 \\ 0.9 \end{bmatrix} \\ &= \begin{bmatrix} 8.0973 \\ -6.4079 \\ 8.7809 \end{bmatrix}. \end{aligned}$$

Summation Block: The summation of 2 Gaussian random variables is also another Gaussian random variable with summed mean and variance values of input random variables. The GMP rules in (2.10)-(2.13) which correspond to the summation block given in Fig. 2.4 uses this principle. The direction of the message passing is important since the summation operation has also its own direction, i.e. $\mathbf{z} = \mathbf{x} + \mathbf{y}$. Hence, the GMP rules through forward direction (following the same direction as the arrows from left to right) are given in (2.10) and (2.12) whereas the GMP rules through backward direction (following the opposite direction of the arrows from right to left) are given in (2.11)-(2.13).

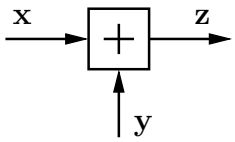

Figure 2.4: Basic Building Blocks-Summation

Example 2: Assume that the information related to state vectors $\mathbf{x}$ and $\mathbf{y}$ are given by the same values as in Example 1 and we need to reach output information related to $\mathbf{z}$, i.e. we go through forward direction. Using (2.10) and (2.12), we can obtain

$$\begin{aligned}\overrightarrow{\mathbf{V}}_{\mathbf{z}} &= \begin{bmatrix} 0.3 & -0.01 & 0.02 \\ -0.01 & 0.25 & 0.05 \\ 0.02 & 0.05 & 0.35 \end{bmatrix} + \begin{bmatrix} 0.27 & 0.07 & -0.03 \\ 0.07 & 0.4 & 0.06 \\ -0.03 & 0.06 & 0.22 \end{bmatrix} \\ &= \begin{bmatrix} 0.57 & 0.06 & -0.01 \\ 0.06 & 0.65 & 0.11 \\ -0.01 & 0.11 & 0.57 \end{bmatrix},\end{aligned}$$

$$\begin{aligned}\overrightarrow{\mathbf{m}}_{\mathbf{z}} &= \begin{bmatrix} 1.3 \\ -0.9 \\ 1.1 \end{bmatrix} + \begin{bmatrix} 0.8 \\ -0.3 \\ 0.9 \end{bmatrix} \\ &= \begin{bmatrix} 2.1 \\ -1.2 \\ 2 \end{bmatrix}.\end{aligned}$$

Scaling Block: The scaling of a Gaussian random variable is also another Gaussian random variable with scaled mean and variance values of the input random variable. The GMP rules in (2.14)-(2.17) which correspond to the scaling block given in Fig. 2.5 uses this principle. The direction of the message passing is important since the scaling operation has also its own direction, i.e. $\mathbf{y} = \mathbf{A}\mathbf{x}$. Hence, the GMP rules through forward direction (following the same direction as the arrows from left to right) are given in (2.14) and (2.15) whereas the GMP rules through backward direction (following the opposite direction of the arrows from right to left) are given in (2.16)-(2.17).

Example 3: Assume that the information related to state vector $\mathbf{x}$ is given by the same

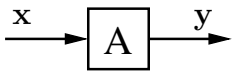

Figure 2.5: Basic Building Blocks-Scaling

values as in Example 1, $\mathbf{A}$ is given by

$$\mathbf{A} = \begin{bmatrix} 0 & 1 & 0 \\ 0 & 0 & 1 \\ 0 & 0 & 0 \end{bmatrix}$$

and we need to reach output information related to $\mathbf{y}$, i.e. we go through forward direction. Using (2.14) and (2.15), we can obtain

$$\begin{aligned} \overrightarrow{\mathbf{m}}_{\mathbf{y}} &= \begin{bmatrix} 0 & 1 & 0 \\ 0 & 0 & 1 \\ 0 & 0 & 0 \end{bmatrix} \begin{bmatrix} 1.3 \\ -0.9 \\ 1.1 \end{bmatrix} \\ &= \begin{bmatrix} -0.9 \\ 1.1 \\ 0 \end{bmatrix}, \end{aligned}$$

$$\begin{aligned} \overrightarrow{\mathbf{V}}_{\mathbf{y}} &= \begin{bmatrix} 0 & 1 & 0 \\ 0 & 0 & 1 \\ 0 & 0 & 0 \end{bmatrix} \begin{bmatrix} 0.3 & -0.01 & 0.02 \\ -0.01 & 0.25 & 0.05 \\ 0.02 & 0.05 & 0.35 \end{bmatrix} \begin{bmatrix} 0 & 1 & 0 \\ 0 & 0 & 1 \\ 0 & 0 & 0 \end{bmatrix}^{H} \\ &= \begin{bmatrix} 0.25 & 0.05 & 0 \\ 0.05 & 0.35 & 0 \\ 0 & 0 & 0 \end{bmatrix}. \end{aligned}$$

Those rules corresponding to basic building blocks given in Table 2.1 could be directly applied to the graph in Fig. 2.2. However, the direct application results in quite a few L-size matrix inversions each of which costs $O(L^3)$ because of the necessary transitions between variance and weight matrices. Hence, we also present the GMP rules for composite blocks with reduced computational complexity by use of matrix inversion lemma [21] in Table 2.2.

Using the given GMP rules in Table 2.1-2.2, forward and backward recursion algorithms can be performed through either mean and variance values or weighted mean

Table2.2: GMP Rules for Composite Blocks with Reduced Computation

Blocks	GMP Rules
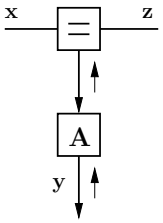	$\overrightarrow{\mathbf{V}}_{\mathbf{z}} = \overrightarrow{\mathbf{V}}_{\mathbf{x}} - \overrightarrow{\mathbf{V}}_{\mathbf{x}}\mathbf{A}^H\mathbf{B}\mathbf{A}\overrightarrow{\mathbf{V}}_{\mathbf{x}}$ (2.18) $\overrightarrow{\mathbf{m}}_{\mathbf{z}} = \overrightarrow{\mathbf{m}}_{\mathbf{x}} + \overrightarrow{\mathbf{V}}_{\mathbf{x}}\mathbf{A}^H\mathbf{B}(\mathbf{m}_{\mathbf{y}}^{\uparrow} - \mathbf{A}\overrightarrow{\mathbf{m}}_{\mathbf{x}})$ (2.19) where $\mathbf{B} = (\mathbf{V}_{\mathbf{y}}^{\uparrow} + \mathbf{A}\overrightarrow{\mathbf{V}}_{\mathbf{x}}\mathbf{A}^H)^{-1}$ (2.20)
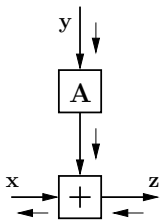	$\overleftarrow{\mathbf{W}}_{\mathbf{x}} = \overleftarrow{\mathbf{W}}_{\mathbf{z}} - \overleftarrow{\mathbf{W}}_{\mathbf{z}}\mathbf{A}\mathbf{C}\mathbf{A}^H\overleftarrow{\mathbf{W}}_{\mathbf{z}}$ (2.21) $\overleftarrow{\mathbf{W}}_{\mathbf{x}}\overleftarrow{\mathbf{m}}_{\mathbf{x}} = (\mathbf{I} - \overleftarrow{\mathbf{W}}_{\mathbf{z}}\mathbf{A}\mathbf{C}\mathbf{A}^H)*$ $(\overleftarrow{\mathbf{W}}_{\mathbf{z}}\overleftarrow{\mathbf{m}}_{\mathbf{z}} - \overleftarrow{\mathbf{W}}_{\mathbf{z}}\mathbf{A}\mathbf{m}_{\mathbf{y}}^{\downarrow})$ (2.22) where $\mathbf{C} = (\mathbf{W}_{\mathbf{y}}^{\downarrow} + \mathbf{A}^H\overleftarrow{\mathbf{W}}_{\mathbf{z}}\mathbf{A})^{-1}$ (2.23)

and weight values of the state variables. Therefore, it is possible to choose one among different configuration pairs. A brief description of the forward and backward recursion algorithms which we use through our study is provided below for the k^{th} building block. The arrows are used so as to show the direction of the messages in a similar notation to [17, 27–29].

- ***Forward Recursion:*** We aim to reach the information related to the state $\overline{\mathbf{x}}_{k+1}$ by use of the known values of the state $\overline{\mathbf{x}}_k$ obtained by the previous building block and the operations given below. Following the direction from left to right on the k^{th} building block of the graph in Fig. 2.2, we compute $\overrightarrow{\mathbf{m}}_{\overline{\mathbf{x}}_k''}$ and $\overrightarrow{\mathbf{V}}_{\overline{\mathbf{x}}_k''}$ by using $\overrightarrow{\mathbf{m}}_{\overline{\mathbf{x}}_k}$, $\overrightarrow{\mathbf{V}}_{\overline{\mathbf{x}}_k}$ coming from the previous building block and the observation y_k through (2.18)-(2.19). As the next step for the calculation of $\overrightarrow{\mathbf{m}}_{\mathbf{z}_{k+1}}$ and $\overrightarrow{\mathbf{V}}_{\mathbf{z}_{k+1}}$, we use (2.14)-(2.15). With the obtained $\overrightarrow{\mathbf{m}}_{\mathbf{z}_{k+1}}$, $\overrightarrow{\mathbf{V}}_{\mathbf{z}_{k+1}}$ values and the *a priori* information provided by the APP decoder $(\mathbf{m}_{\mathbf{x}_{k+1}}^{\downarrow}, \mathbf{V}_{\mathbf{x}_{k+1}}^{\downarrow})$, the mean and variance values of the state vector $\overline{\mathbf{x}}_{k+1}$ are computed by (2.10),(2.12),(2.14), (2.15) and used in the next building block as input. By repeating this process for all the building blocks in a serial order, forward recursion is completed.

- ***Backward Recursion:*** In each building block, the purpose is to obtain the weight matrix $\overleftarrow{\mathbf{W}}_{\overline{\mathbf{x}}_k}$ and the weighted mean vector $\overleftarrow{\mathbf{W}}_{\overline{\mathbf{x}}_k}\overleftarrow{\mathbf{m}}_{\overline{\mathbf{x}}_k}$ of the state $\overline{\mathbf{x}}_k$

from the known information related to state $\overline{\mathbf{x}}_{k+1}$ provided by the previous building block. Following the direction from right to left on the k^{th} building block, first we compute $\overleftarrow{\mathbf{W}}_{\mathbf{z}_{k+1}}$, $\overleftarrow{\mathbf{W}}_{\mathbf{z}_{k+1}}\overleftarrow{\mathbf{m}}_{\mathbf{z}_{k+1}}$ through (2.21)-(2.22) with the help of the *a priori* information coming from the APP decoder ($\mathbf{m}^{\downarrow}_{\mathbf{x}_{k+1}}$, $\mathbf{V}^{\downarrow}_{\mathbf{x}_{k+1}}$) and the obtained information of the state $\overline{\mathbf{x}}_{k+1}$ ($\overleftarrow{\mathbf{W}}_{\overline{\mathbf{x}}_{k+1}}$, $\overleftarrow{\mathbf{W}}_{\overline{\mathbf{x}}_{k+1}}\overleftarrow{\mathbf{m}}_{\overline{\mathbf{x}}_{k+1}}$) by the previous building block. Then, after $\overleftarrow{\mathbf{W}}_{\overline{\mathbf{x}}''_k}$ and $\overleftarrow{\mathbf{W}}_{\overline{\mathbf{x}}''_k}\overleftarrow{\mathbf{m}}_{\overline{\mathbf{x}}''_k}$ are computed by (2.16)-(2.17), they are utilized in (2.10)-(2.12), (2.16)-(2.17) together with the observation y_k so as to reach $\overleftarrow{\mathbf{W}}_{\overline{\mathbf{x}}_{k+1}}$, $\overleftarrow{\mathbf{W}}_{\overline{\mathbf{x}}_{k+1}}\overleftarrow{\mathbf{m}}_{\overline{\mathbf{x}}_{k+1}}$. These operations are applied to each building block serially in a way similar to forward recursion.

When forward and backward recursions are complete, *a posteriori* mean vector and covariance matrix of each state vector $\overline{\mathbf{x}}_k$ are calculated with the help of the obtained ($\overrightarrow{\mathbf{V}}_{\overline{\mathbf{x}}_k}, \overrightarrow{\mathbf{m}}_{\overline{\mathbf{x}}_k}$) and ($\overleftarrow{\mathbf{W}}_{\overline{\mathbf{x}}_k}, \overleftarrow{\mathbf{W}}_{\overline{\mathbf{x}}_k}\overleftarrow{\mathbf{m}}_{\overline{\mathbf{x}}_k}$) as in [26], [17]:

$$\mathbf{V}^{post}_{\overline{\mathbf{x}}_k} = (\overrightarrow{\mathbf{V}}^{-1}_{\overline{\mathbf{x}}_k} + \overleftarrow{\mathbf{W}}_{\overline{\mathbf{x}}_k})^{-1} \tag{2.24}$$

$$\mathbf{m}^{post}_{\overline{\mathbf{x}}_k} = \mathbf{V}^{post}_{\overline{\mathbf{x}}_k}(\overrightarrow{\mathbf{V}}^{-1}_{\overline{\mathbf{x}}_k}\overrightarrow{\mathbf{m}}_{\overline{\mathbf{x}}_k} + \overleftarrow{\mathbf{W}}_{\overline{\mathbf{x}}_k}\overleftarrow{\mathbf{m}}_{\overline{\mathbf{x}}_k})^{-1}. \tag{2.25}$$

The elements of $\mathbf{m}^{post}_{\overline{\mathbf{x}}_k}$ determine the *a posteriori* mean values of the transmitted symbols while the diagonal elements of $\mathbf{V}^{post}_{\overline{\mathbf{x}}_k}$ provide the *a posteriori* variance values of the transmitted symbols between the time instants $k-J$ and k as given by

$$\mathbf{m}^{post}_{\overline{\mathbf{x}}_k} = \begin{bmatrix} m^{post}_{x_{k-J}} \\ m^{post}_{x_{k-J+1}} \\ \vdots \\ m^{post}_{x_k} \end{bmatrix}, \quad \mathbf{V}^{post}_{\overline{\mathbf{x}}_k} = \begin{bmatrix} v^{post}_{x_{k-J}} & \dots & \dots \\ \dots & v^{post}_{x_{k-J+1}} & \dots \\ \dots & \ddots & \dots \\ \dots & \dots & v^{post}_{x_k} \end{bmatrix}. \tag{2.26}$$

Since the elements of the state vector $\overline{\mathbf{x}}_k$ are shifted by 1 symbol through the way to $\overline{\mathbf{x}}_{k+1}$, this shift is also seen at the output mean vectors and variance matrices as

$$\mathbf{m}^{post}_{\overline{\mathbf{x}}_{k+1}} = \begin{bmatrix} m^{post}_{x_{k-J+1}} \\ m^{post}_{x_{k-J+2}} \\ \vdots \\ m^{post}_{x_{k+1}} \end{bmatrix}, \quad \mathbf{V}^{post}_{\overline{\mathbf{x}}_{k+1}} = \begin{bmatrix} v^{post}_{x_{k-J+1}} & \dots & \dots \\ \dots & v^{post}_{x_{k-J+2}} & \dots \\ \dots & \ddots & \dots \\ \dots & \dots & v^{post}_{x_{k+1}} \end{bmatrix}. \tag{2.27}$$

The major contribution to the complexity of the presented algorithm on the graph structure is caused by the matrix inversions in (2.24)-(2.25). However, matrix inversions need to be applied only once for every L building blocks with a complexity of $O(L^3)$ owing to the shifting property of the state vectors as explained in (2.27). Hence, complexity reduces to $O(L^2)$ for each building block, i.e., each time instant, while there are N building blocks in our system. Therefore, the overall complexity is approximately $O(NL^2)$. As a result of this discussion, the overall complexity per symbol per transmit antenna is about $O(L^2)$ which is reasonably lower than both the block LMMSE filtering operation and the other time domain equalizer structures mentioned in Chapter 1.

An algorithm is needed for transition between the Gaussian and binary bit LLR domains which is given in the next section.

2.2.3 LLR Exchange Algorithm

Using the LMMSE equalizer, which accepts inputs and generates outputs in the form of mean and variance values in an iterative receiver, requires transition between Gaussian and binary domains. For transition from the LLR domain at the output of the APP decoder to the Gaussian domain of the LMMSE equalizer, *a priori* mean and variance of each transmitted symbol is obtained by [17]

$$m_{x_k}^{\downarrow} = \sum_{s_i \in S} s_i P(x_k = s_i), \tag{2.28}$$

$$v_{x_k}^{\downarrow} = \sum_{s_i \in S} |s_i - m_{x_k}^{\downarrow}|^2 P(x_k = s_i), \tag{2.29}$$

where S denotes the modulation alphabet and $P(x_k = s_i)$'s represent the *a priori* probabilities to the LMMSE equalizer related to the k^{th} transmitted symbol obtained by LLRs at the output of the APP decoder.

However, the transition from LMMSE equalizer to APP decoder is not so standard. There are proposed mathematical models for the extrinsic bit LLR computation of the LMMSE equalizer in the literature such as the Wang-Poor [40, 42] and the Joint Gaussian (JG) approaches [25], which are not suitable for the graph based LMMSE equalization due to their high computational complexity of $O(N^3)$ caused by ma-

trix inversions. In [17], considering the graph outputs, the mathematical expression of the extrinsic bit LLRs with respect to the JG approach was simplified for BPSK signaling. Also, the authors of [17] show the equivalence between the JG and Wang-Poor approaches for BPSK signaling. However, there is no mathematically justified reduced complexity LLR exchange algorithm for higher constellation sizes in the literature to the best of our knowledge. Although [16] proposes an intuitive method for M-QAM signaling without any simulation results, we have observed that the equation (8) in [16] causes both diversity and SNR losses as to be shown in Section 2.3. Moreover, we have also proposed a heuristic algorithm in which both the intrinsic and the *a priori* LLRs are computed under the Gaussian assumption in [38]. Although it has much better performance than the one in [16] for M-QAM signaling, there exists no scientifically proved basis for the idea behind our heuristic method. Hence, we provide the simplified mathematical relation between the graph based LMMSE equalizer outputs (*a posteriori* mean and variance values) and the bit LLRs for higher order modulation alphabets with respect to the widely known Wang Poor approach, which is observed to have the best performance among the mentioned approaches. Owing to this key connection, extrinsic bit LLR values from the LMMSE estimation can be obtained easily in accordance with the graph solution without any major complexity increase. In the following sections, this extrinsic LLR computation method with respect to the Wang Poor approach will be used due to its better performance.

According to the Wang-Poor approach, Gaussian approximation is held after the LMMSE equalization process [40, 42]. In other words, the residual interference plus noise term at the output of the LMMSE equalizer can be well approximated by Gaussian distribution. Hence, the filtered observation at time k $(\hat{x}_k)$ given an input symbol is assumed to have Gaussian distribution, i.e., the probability density function (pdf) of $p(\hat{x}_k|x_k = s) \sim N(\mu_k s, \sigma_k)$ with $s \in S$. An equivalent model for this approximation can be written similarly to [42] as

$$\hat{x}_k = \mu_k \, x_k + \eta_k, \tag{2.30}$$

where $\eta_k \sim N(0, \sigma_k)$. To reach the extrinsic information, [40] rearranges the expression of the filtered observation at time k by setting $m_{x_k}^{prio} = 0$ and $v_{x_k}^{prio} = 1$ so that it

does not depend on the current *a priori* information $(m_{x_k}^{prio}, v_{x_k}^{prio})$, which gives

$$\hat{x}_k = \mathbf{w}_k^H(\mathbf{y} - \mathbf{H}\mathbf{m}_{\mathbf{x}}^{prio} + m_{x_k}^{prio}\,\mathbf{h}_k) \tag{2.31}$$

where $\mathbf{h}_k$ is the k^{th} column of the channel convolution matrix $\mathbf{H}$ with size $(N{+}J)\times N$, and $\mathbf{w}_k$ is the LMMSE filter coefficient vector with length $N+J$ for the k^{th} input symbol as expressed by

$$\mathbf{w}_k = (N_0\mathbf{I}_{N+J} + \sum_{\substack{i=1\\ i\neq k}}^{N} v_{x_i}^{prio}\mathbf{h}_i\mathbf{h}_i^H + \mathbf{h}_k\mathbf{h}_k^H)^{-1}\mathbf{h}_k \tag{2.32}$$

and, μ_k and σ_k are obtained in [40] as

$$\mu_k = \mathbf{w}_k^H\,\mathbf{h}_k \tag{2.33}$$

$$\sigma_k^2 = \mathbf{w}_k^H\,\mathbf{h}_k(1 - \mathbf{h}_k^H\,\mathbf{w}_k) \tag{2.34}$$

$$= \mu_k(1 - \mu_k^H). \tag{2.35}$$

If the k^{th} transmitted symbol is represented by b bits of $[c_{k,1}\ c_{k,2}\ \ldots\ c_{k,b}]$, then the extrinsic LLR value of the q^{th} bit of the k^{th} symbol could be expressed by

$$L_E(c_{k,q}) = \ln\left(\frac{\sum_{s\in S_{q,0}} p(x_k = s|\hat{x}_k)}{\sum_{s\in S_{q,1}} p(x_k = s|\hat{x}_k)}\right) - \ln\left(\frac{\sum_{s\in S_{q,0}} p(x_k = s)}{\sum_{s\in S_{q,1}} p(x_k = s)}\right) \quad q = 1, 2, \ldots, b \tag{2.36}$$

where $S_{q,0}$ $(S_{q,1})$ denotes the subset of the modulation alphabet S with symbols whose q^{th} bit is 0 (1) and $p(x_k = s)$'s are the *a priori* symbol probabilities. Using Bayes Rule [6], (2.36) can be rewritten by considering the Gaussian assumption in (2.30) as

$$L_E(c_{k,q}) = \ln\left(\frac{\sum_{s\in S_{q,0}} p(\hat{x}_k|x_k = s)p(x_k = s)}{\sum_{s\in S_{q,1}} p(\hat{x}_k|x_k = s)p(x_k = s)}\right) - \ln\left(\frac{\sum_{s\in S_{q,0}} p(x_k = s)}{\sum_{s\in S_{q,1}} p(x_k = s)}\right) \quad q = 1, 2, \ldots, b \tag{2.37}$$

where

$$p(\hat{x}_k|x_k = s) \propto \exp(-|\hat{x}_k - \mu_k s|^2/\sigma_k^2). \tag{2.38}$$

We also use the following approximated version of (2.37) in our simulations to further reduce its complexity.

$$L_E(c_{k,q}) \propto \ln\left(\frac{\sum_{s\in S_{q,0}} p(\hat{x}_k|x_k = s)}{\sum_{s\in S_{q,1}} p(\hat{x}_k|x_k = s)}\right) \quad q = 1, 2, \ldots, b \tag{2.39}$$

It should be noted that (2.39) is equal to (2.37) for BPSK signalling. For M-QAM signalling, the comparative performance results of (2.37) and (2.39) will be presented in the related sections of other chapters which include simulation results.

As can be seen in (2.31)-(2.35), the complexity of finding $\hat{x}_k$, μ_k and σ_k values is $O(N^3)$ and mainly determined by (2.32), which involves a matrix inversion of size $(N+J) \times (N+J)$. Moreover, there is no mathematical simplification in the extrinsic bit LLR expression in (2.37) for M-QAM signalling due to the summation over symbols unlike the BPSK signalling case discussed in [17]. Hence, this version of Wang-Poor approach is not suitable for the graph based LMMSE equalization. The propositions below provide the key connection between the graph outputs (*a posteriori* mean and variance values) and the Wang-Poor parameters ($\hat{x}_k$, μ_k and σ_k) with no major complexity increase.

- **Proposition 1**:

$$\hat{x}_k = \left(\frac{m_{x_k}^{post}}{v_{x_k}^{post}} - \frac{m_{x_k}^{prio}}{v_{x_k}^{prio}} \right) / \left(1 + \frac{1}{v_{x_k}^{post}} - \frac{1}{v_{x_k}^{prio}} \right) \tag{2.40}$$

- **Proposition 2**:

$$\frac{\mu_k}{\sigma_k^2} = \left(1 + \frac{1}{v_{x_k}^{post}} - \frac{1}{v_{x_k}^{prio}} \right) \tag{2.41}$$

  With the help of (2.35) and (2.40)-(2.41), the parameters of Wang-Poor approach, so the extrinsic bit LLRs, related to each transmitted symbol are easily computed by applying simple operations to the graph outputs.

- **Proof of Propositions 1-2**: The LMMSE filter coefficient vector for the k^{th} transmitted symbol, $\mathbf{w}_k$, previously given in (2.32) can be rewritten as

$$\mathbf{w}_k = \left(\mathbf{V}_{\xi_k} + \mathbf{h}_k \mathbf{h}_k^H \right)^{-1} \mathbf{h}_k, \quad \text{where} \tag{2.42}$$

$$\mathbf{V}_{\xi_k} \triangleq N_0 \mathbf{I}_{N+J} + \sum_{\substack{i=1 \\ i \neq k}}^{N} v_{x_i}^{prio} \mathbf{h}_i \mathbf{h}_i^H. \tag{2.43}$$

  By matrix inversion lemma [21], (2.42) is simplified to

$$\mathbf{w}_k = \frac{\mathbf{V}_{\xi_k}^{-1} \mathbf{h}_k}{1 + \mathbf{h}_k^H \mathbf{V}_{\xi_k}^{-1} \mathbf{h}_k}. \tag{2.44}$$

  Inserting (2.44) into (2.31) gives

$$\hat{x}_k = \frac{\mathbf{h}_k^H \mathbf{V}_{\xi_k}^{-1}}{1 + \mathbf{h}_k^H \mathbf{V}_{\xi_k}^{-1} \mathbf{h}_k} \left(\mathbf{y} - \mathbf{H} \mathbf{m}_{\mathbf{x}}^{prio} + \mathbf{h}_k m_{x_k}^{prio} \right). \tag{2.45}$$

The outputs of the LMMSE equalizer, the *a posteriori* mean and variance values, are defined in [22] and used in [17] as

$$v_{x_k}^{post} = \frac{1}{1/v_{x_k}^{prio} + \mathbf{h}_k^H \mathbf{V}_{\xi_k}^{-1} \mathbf{h}_k} \tag{2.46}$$

$$m_{x_k}^{post} = \frac{m_{x_k}^{prio}/v_{x_k}^{prio} + \mathbf{h}_k^H \mathbf{V}_{\xi_k}^{-1} \left(\mathbf{y} - \mathbf{H}\mathbf{m}_{\mathbf{x}}^{prio} + \mathbf{h}_k m_{x_k}^{prio}\right)}{1/v_{x_k}^{prio} + \mathbf{h}_k^H \mathbf{V}_{\xi_k}^{-1} \mathbf{h}_k}. \tag{2.47}$$

Using (2.45)-(2.47) we obtain

$$\begin{aligned}\left(\frac{m_{x_k}^{post}}{v_{x_k}^{post}} - \frac{m_{x_k}^{prio}}{v_{x_k}^{prio}}\right) =& \mathbf{h}_k^H \mathbf{V}_{\xi_k}^{-1} \left(\mathbf{y} - \mathbf{H}\mathbf{m}_{\mathbf{x}}^{prio} + \mathbf{h}_k m_{x_k}^{prio}\right) \\ =& \hat{x}_k \left(1 + \mathbf{h}_k^H \mathbf{V}_{\xi_k}^{-1} \mathbf{h}_k\right). \end{aligned} \tag{2.48}$$

Combining (2.46) and (2.48) provides the proposition for $\hat{x}_k$ in (2.40) as seen by

$$\begin{aligned}\hat{x}_k &= \left(\frac{m_{x_k}^{post}}{v_{x_k}^{post}} - \frac{m_{x_k}^{prio}}{v_{x_k}^{prio}}\right) / \left(1 + \mathbf{h}_k^H \mathbf{V}_{\xi_k}^{-1} \mathbf{h}_k\right) \\ &= \left(\frac{m_{x_k}^{post}}{v_{x_k}^{post}} - \frac{m_{x_k}^{prio}}{v_{x_k}^{prio}}\right) / \left(1 + \frac{1}{v_{x_k}^{post}} - \frac{1}{v_{x_k}^{prio}}\right). \end{aligned} \tag{2.49}$$

In order to derive the proposition given in (2.41), we use (2.33) and (2.34) so that the relation between σ_k and μ_k is obtained as

$$\frac{\sigma_k^2}{\mu_k} = 1 - \mathbf{h}_k^H \mathbf{w}_k. \tag{2.50}$$

Inserting the expression for $\mathbf{w}_k$ in (2.44) to (2.50) gives

$$\frac{\mu_k}{\sigma_k^2} = 1 + \mathbf{h}_k^H \mathbf{V}_{\xi_k}^{-1} \mathbf{h}_k. \tag{2.51}$$

Using (2.46) and (2.51), we get

$$1 + \mathbf{h}_k^H \mathbf{V}_{\xi_k}^{-1} \mathbf{h}_k = 1 + \frac{1}{v_{x_k}^{post}} - \frac{1}{v_{x_k}^{prio}}. \tag{2.52}$$

The derivations given above provide a mathematical transition between the LMMSE equalizer outputs and the commonly used Wang-Poor approach for the extrinsic LLR calculation, which is very useful particularly for the graph based LMMSE algorithms for M-QAM modulation.

2.3 Simulation Results

The performance comparison among the heuristic extrinsic LLR calculation method, which we proposed in [38], the one proposed in [16] and the simplified forms of Wang Poor approach by (2.37) and (2.39) explained in Section 2.2.3 is shown in Fig. 2.6. For all methods, the LMMSE equalizer in [17] is implemented for a 6-tap static ISI pattern of $[0.408\ 0\ 0\ 0\ 0.816\ 0.408]$, which is taken from [10] under white Gaussian noise with Gray encoded 64-QAM signaling. The data length is set to 1800 uncoded bits. A convolutional code with code rate $1/2$ and generator polynomial $[133\ 171]$ is used. The number of iterations is 5. It is observed by trial and error that multiplying the LLR values exchanged between the decoder and the equalizer by scaling factors (less than 1) improves the BER performance, since it prevents overconfidence in LLR messages. Similar methods are also applied in [8, 9, 14, 19, 32] for turbo equalization and decoding structures. Here, we multiply the extrinsic LLR values produced with respect to [38] at the output of the LMMSE equalizer by the scaling factor of 0.5. For the methods in [16] and the ones explained in Section 2.2.3, no enhancement is observed in performance with the help of a scaling factor through simulations for the presented scenario. Therefore, we do not perform any scaling operation for them.

We also provide the performance under a 1-tap AWGN channel with the same simulation details as the ISI channel scenario to put an upper bound. To obtain this performance, the APP decoder is operated only once by using the bit LLR values which are generated from the conditional probabilities given each of 64 points in the constellation for each input symbol. This is a non-iterative receiver which we call as "AWGN" in Fig. 2.6. The explicit computation of the LLR value of the q^{th} bit of kth symbol entered to the APP decoder L_{AWGN} is

$$L_{AWGN}(c_{k,q}) = \ln\left(\frac{\sum_{s\in S_{q,0}} p(y_k|x_k=s)}{\sum_{s\in S_{q,1}} p(y_k|x_k=s)}\right) \quad q=1,2,\ldots,b \tag{2.53}$$

where

$$p(y_k|x_k=s)\exp(-|y_k-s|^2/N_0) \tag{2.54}$$

and $S_{q,0}$ $(S_{q,1})$ denotes the subset of the modulation alphabet S with symbols whose q^{th} bit is 0 (1).

It should be noted that we have observed non-ignorable performance gain (about 1 dB as seen from Fig. 2.6) if the explained LMMSE receiver structure is used with 3 turbo iterations for the mentioned 1-tap channel under 64-QAM signalling since its performance improves through turbo iterations. The performance of the receiver called AWGN corresponds to 1^{st} iteration performance of LMMSE receiver. The reason for the improving effect of turbo iterations is to use the bit interleaved coded modulation even if there is no fading channel. Although this phenomenon is not observed with smaller constellation sizes (there is no improvement resulted from turbo iterations for 16-QAM and smaller constellation sizes), turbo decoding becomes important in 64-QAM where there are 6 bits in 1 symbol.

It is seen at 10^{-4} BER level that there is more than 4 dB and nearly 2 dB gain of our method using (2.37) with respect to the ones in [16] and [38] respectively. The approximated version of exact implementation of Wang Poor (WP) in (2.37) was given in (2.39) which has a performance loss of 1 dB as compared to (2.37) and is still better than other methods. Another important point to mention is that the method in [16] leads to no improvement in performance as the number of turbo iterations increases. Hence, the Wang Poor approach with the simplified version for the factor graph structures is seen to be the best choice for M-QAM modulation among the other proposed solutions. Therefore, we use this method for the LLR computation in the rest of our study.

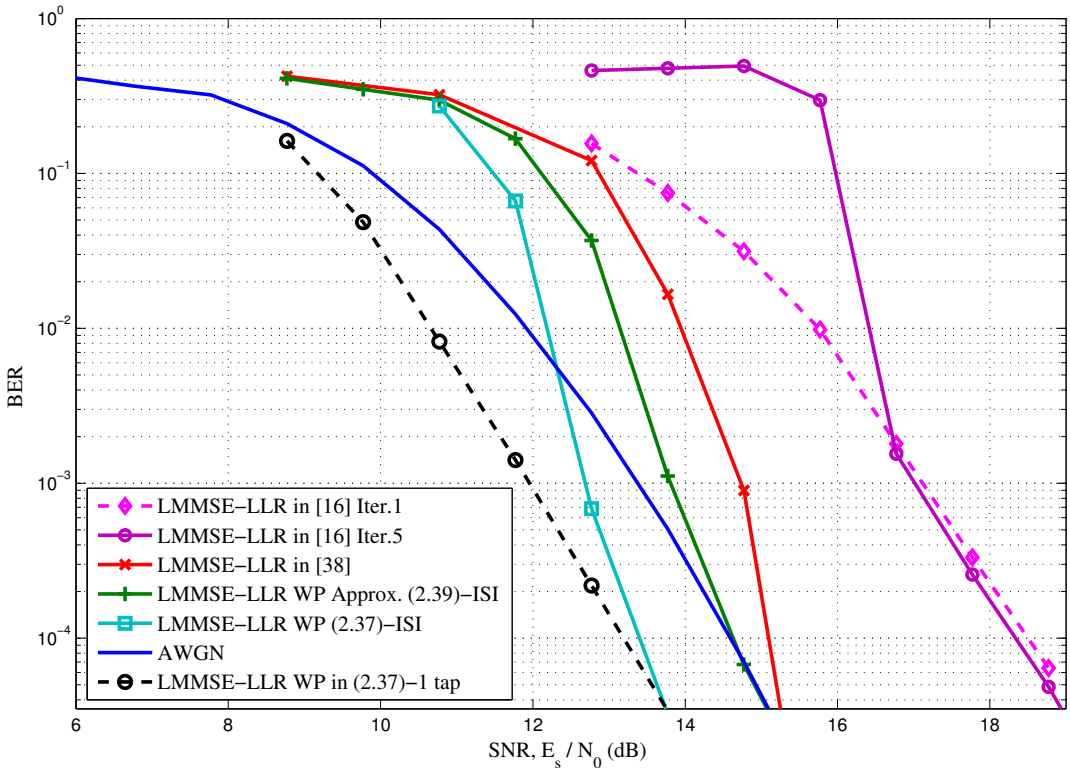

Figure 2.6: Performance comparison of the extrinsic bit LLR calculation methods for LMMSE filtering under 64-QAM signaling

CHAPTER 3

FACTOR GRAPH BASED LMMSE FILTERING GENERALIZED TO COLORED GAUSSIAN PROCESSES FOR SISO ISI CHANNELS

In this section, we modify the factor graph structure presented in Chapter 2 under white Gaussian noise for colored Gaussian processes so that the non-white statistics of a random process are taken into account. The presented method here still preserves the advantages of having a complexity linearly increasing with the block length and the ease of incorporating the *a priori* information of the input signals whenever possible. First, we show that the proposed graph based algorithm under SISO ISI channels corresponds to conventional block LMMSE filtering for an AR Gaussian process through extensive Monte Carlo simulations and the theoretical MSE values. Then, we will present an approximation to an AR process so that it can be used with any random process with a known (or estimated) autocorrelation function.

3.1 Factor Graph Based LMMSE Filtering for AR Gaussian Processes

We aim to obtain a reduced complexity graph based LMMSE filtering operation which has the ability of including the statistics of the non-white Gaussian noise. Hence, we start with the Gaussian domain where the optimal solution is the block LMMSE filtering so as to provide comparative mean square error (MSE) performances. First we present previously studied graph based LMMSE filter structure which is applicable for any kind of stationary noise process resulting in a complexity $O(N^3)$. Then we will introduce our proposed reduced complexity graph structure

together with the comparative performance results.

3.2 System Model

We consider the system given in Fig. 3.1. The source sequence $\{x(k)\}$ is generated

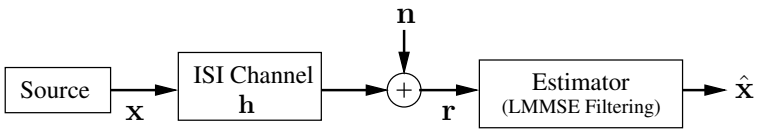

Figure 3.1: System Model in Gaussian Domain

according to a white ZMCSCG process with variance 1, i.e., $x(k) \sim CN(0,1)$ and the noise sequence $\{n(k)\}$ is generated according to a p^{th} order AR process as defined in [7]

$$n(k) = \sum_{j=1}^{p} a(j)n(k-j) + w(k), \tag{3.1}$$

where $w(k)$ is a white ZMCSCG process with variance σ_w^2, i.e., $w(k) \sim CN(0, \sigma_w^2)$, and $a(j)$'s are known AR process parameters. The multipath channel effect which is a commonly observed problem in wireless communications can be included in the system model via an ISI channel gain vector of $\mathbf{h}$ with L taps. Then, the noisy observation $r(k)$ at time k is

$$r(k) = \sum_{i=0}^{L-1} h(i)x(k-i) + n(k) \quad k = 1, 2, \ldots, N+L-1 \tag{3.2}$$

where N is the length of the input sequence, E_s is defined as the average received signal energy, i.e. $E_s \triangleq \sum_{i=0}^{L-1} E\{|h(i)|^2\}$ and N_0 is defined as the variance of the zero-mean noise process, i.e., $N_0 \triangleq E\{|n(k)|^2\}$. Parameters N_0, $a(j)$'s and σ_w^2 are related by Yule-Walker equations [7] as

$$R_n(j) = \begin{cases} \sum_{i=1}^{p} a(i)R_n(-i) + \sigma_w^2 & \text{for } j = 0 \\ \sum_{i=1}^{p} a(i)R_n(j-i) & \text{for } j > 0, \end{cases} \tag{3.3}$$

where $R_n(j)$ denotes the samples of the autocorrelation function of the AR noise process n, i.e., $R_n(j) \triangleq E\{n(k)n(k+j)^*\}$ and $N_0 = R_n(0)$. Therefore, we keep N_0 constant by adjusting $a(j)$'s and σ_w^2 accordingly.

The system described by (3.2) can also be written by matrix representation as follows

$$\mathbf{r} = \mathbf{H}\mathbf{x} + \mathbf{n}, \tag{3.4}$$

$$\mathbf{H} = \begin{bmatrix} h(0) & 0 & 0 & \dots & 0 \\ \vdots & h(0) & 0 & \dots & 0 \\ h(L-1) & \dots & h(0) & \ddots & \vdots \\ 0 & \ddots & & \ddots & 0 \\ \vdots & \ddots & h(L-1) & \dots & h(0) \\ 0 & \dots & 0 & \ddots & \vdots \\ 0 & \dots & 0 & 0 & h(L-1) \end{bmatrix}. \tag{3.5}$$

where $\mathbf{H}$ is the convolution matrix of size $(N + J) \times N$ originating from the ISI pattern of length L and J is defined as the channel memory, i.e. $J \triangleq L - 1$.

3.3 Graph Based LMMSE Filtering for Colored Processes

A graph based LMMSE filter for a system described via (3.4) was previously proposed in [28]. The state space representation for the factor graph shown in Fig. 3.2 which is applicable for any kind of stationary noise process is

$$\mathbf{r} = \sum_{k=1}^{N} \mathbf{b}_k \, x(k) + \mathbf{n}, \tag{3.6}$$

where $\mathbf{b}_k$ denotes the k^{th} column vector of the channel convolution matrix $\mathbf{H}$ and $\mathbf{n}$ denotes the noise vector both of which are length $(N+J)$. Similar to the one in Chapter 2, each branch on this graph corresponds to either a set of state variables in vector form or a scalar state variable. For example, $\mathbf{S}_k$ represents the state variable vector of $(\mathbf{b}_k x(k))$, i.e.,

$$\mathbf{S}_k = [0 \ \dots \ 0 \quad h(0)x(k) \quad h(1)x(k) \quad \dots \quad h(J)x(k) \quad 0 \ \dots \ 0]^T, \tag{3.7}$$

which is non-zero between k^{th} and $(k+J)^{th}$ entries, and $\mathbf{n}$ represents the noise state variable vector of $[n(1) \quad n(2) \ \ldots \ n(N+J)]^T$.

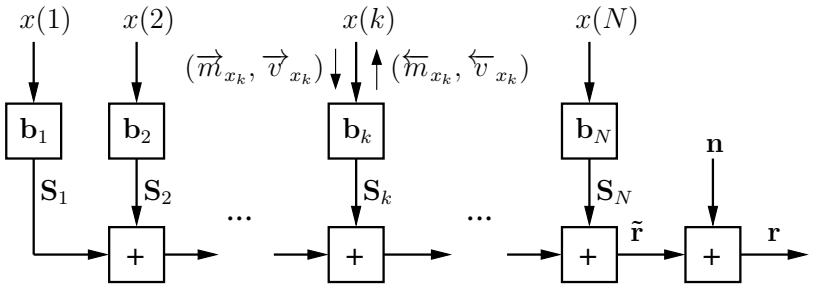

Figure 3.2: General Factor Graph of LMMSE Filtering Operation

The block LMMSE filtering operation is implemented with the help of this graph by applying the GMP rules in [28] which operates on the mean and variance values of the state variables similar to Chapter 2. The main purpose is to calculate the *a posteriori* mean and variance values of the input source sequence by use of the incoming $(\overrightarrow{m}_{x_k}, \overrightarrow{v}_{x_k})$ and outgoing messages $(\overleftarrow{m}_{x_k}, \overleftarrow{v}_{x_k})$ resulting from the forward and backward recursions as [28, 29]

$$v_{x_k}^{post} = (\overrightarrow{v}_{x_k}^{-1} + \overleftarrow{v}_{x_k}^{-1})^{-1}, \tag{3.8}$$

$$m_{x_k}^{post} = v_{x_k}^{post}(\overrightarrow{v}_{x_k}^{-1}\overrightarrow{m}_{x_k} + \overleftarrow{v}_{x_k}^{-1}\overleftarrow{m}_{x_k}). \tag{3.9}$$

The incoming messages $\overrightarrow{m}_{x_k}$ and $\overrightarrow{v}_{x_k}$ are determined by the existing *a priori* information of the input signal and are taken as 0 and 1 respectively in the setting studied here since $x(k) \sim CN(0,1)$; i.e., the source is assumed to generate a white complex Gaussian signal sequence. The outgoing messages $\overleftarrow{m}_{x_k}$ and $\overleftarrow{v}_{x_k}$ are generated by using the GMP rules in [28] with the help of the observation vector $\mathbf{r}$, statistics of the noise process and the incoming messages. First, the auxiliary quantity $\tilde{\mathbf{W}}_{\mathbf{x}}$ defined in [28] for the specified vector $\mathbf{x}$ is written for scalar state variable x_k as

$$\tilde{w}_{x_k} \triangleq (\overleftarrow{v}_{x_k} + \overrightarrow{v}_{x_k})^{-1}. \tag{3.10}$$

Using (3.10) together with the GMP rules which are listed below produces [28]

$$\overleftarrow{v}_{x_k} = \tilde{w}_{x_k}^{-1} - \overrightarrow{v}_{x_k} \tag{3.11}$$

$$= \left(\mathbf{b}_k^H \tilde{\mathbf{W}}_{\mathbf{S}_k} \mathbf{b}_k\right)^{-1} - \overrightarrow{v}_{x_k} \quad \text{and} \tag{3.12}$$

$$\tilde{w}_{x_k} \overleftarrow{m}_{x_k} = \mathbf{b}_k^H \, \tilde{\mathbf{W}}_{\mathbf{S}_k} \overleftarrow{\mathbf{m}}_{\mathbf{S}_k} \tag{3.13}$$

$$\overleftarrow{m}_{x_k} = \left(\mathbf{b}_k^H \tilde{\mathbf{W}}_{\mathbf{S}_k} \mathbf{b}_k\right)^{-1} \mathbf{b}_k^H \tilde{\mathbf{W}}_{\mathbf{S}_k} \overleftarrow{\mathbf{m}}_{\mathbf{S}_k} \tag{3.14}$$

where the information related to the state variable $\mathbf{S}_k$ is

$$\overleftarrow{\mathbf{m}}_{\mathbf{S}_k} = \overleftarrow{\mathbf{m}}_{\tilde{\mathbf{r}}} - \sum_{j=1}^{N} \mathbf{b}_j \overrightarrow{m}_{x_j} + \mathbf{b}_k \overrightarrow{m}_{x_k} \quad \text{and} \tag{3.15}$$

$$\tilde{\mathbf{W}}_{\mathbf{S}_k} = \tilde{\mathbf{W}}_{\tilde{\mathbf{r}}}, \quad \text{for } k = 1, 2, \ldots, N. \tag{3.16}$$

Similar to (3.10), the auxiliary quantity for $\tilde{\mathbf{r}}$ can be written as

$$\tilde{\mathbf{W}}_{\tilde{\mathbf{r}}} \triangleq \left(\overrightarrow{\mathbf{V}}_{\tilde{\mathbf{r}}} + \overleftarrow{\mathbf{V}}_{\tilde{\mathbf{r}}}\right)^{-1}, \tag{3.17}$$

where $\tilde{\mathbf{r}}$ is the noise free observation vector and its covariance matrix in forward direction $\overrightarrow{\mathbf{V}}_{\tilde{\mathbf{r}}}$ is calculated as [28]

$$\overrightarrow{\mathbf{V}}_{\tilde{\mathbf{r}}} = \sum_{j=1}^{N} \mathbf{b}_j \overrightarrow{v}_{x_j} \mathbf{b}_j^H. \tag{3.18}$$

Since noise $n(k)$ is a zero-mean process with the autocorrelation matrix $\mathbf{R}_n$ in our case, mean and covariance of $\tilde{\mathbf{r}}$ are set as $\overleftarrow{\mathbf{m}}_{\tilde{\mathbf{r}}} = \mathbf{r}$ and $\overleftarrow{\mathbf{V}}_{\tilde{\mathbf{r}}} = \mathbf{R_n}$ in (3.15) and (3.17) respectively.

The computational complexity of this algorithm is mainly determined by the matrix inversion in (3.17) and approximately $O(N^3)$ assuming $J \ll N$ since $\overrightarrow{\mathbf{V}}_{\tilde{\mathbf{r}}}$ in (3.17) is an $(N+J)\times(N+J)$ matrix. We use the performance results of this algorithm as a benchmark to those of our proposed reduced complexity graph detailed in the next section.

3.4 Reduced Complexity Graph Structure for LMMSE Filtering under AR Noise Process

The $O(N^3)$ complexity of the algorithm given in Section 3.3 can be decreased to an $O(NL^2)$ complexity under the white noise scenario by separating the observation and noise vectors into scalar elements which is indeed the graph representation explained in Chapter 2. However, this separation does not work under a non-white noise process since the observations conditioned on the input sequence are no longer independent. Hence, there is no work proposing a reduced complexity factor graph for colored noise case to the best of our knowledge.

On the other hand, the authors of [15] discuss the forward Kalman filtering operations under an order-p Gaussian AR noise process and propose to concatenate the set of state variables including the input sequence and the set of noise variables of length p. Hence, the main basis of our method is to apply this idea to the graph based LMMSE filtering operation studied in [17] so as to implement the LMMSE approach having a computational complexity linearly increasing with N under colored noise. In other words, we extend the state variable vector in the graph in [17] which is composed of only the input sequence by joining the noise variables and we make the necessary adjustments to preserve the smooth transition between the building blocks of the graph. This idea is also to be identified in Fig. 3.3 later.

In our graph representation the observation at time k is the same as in (3.2). Hence, the k^{th} element of the observation vector $\mathbf{r}$ in (3.2) can be rewritten as

$$r(k) = \overline{\mathbf{h}}\,\overline{\mathbf{x}}_k, \tag{3.19}$$

where

$$\overline{\mathbf{h}} = [h(J) \ \ldots \ h(1) \quad h(0) \quad 0 \ \ldots \ 0 \ 1]_{(1\times L+p)}, \text{ and} \tag{3.20}$$

$$\overline{\mathbf{x}}_k = [x(k-J) \ \ldots \ x(k-1) \quad x(k) \quad n(k-p+1) \ \ldots \ n(k)]^T. \tag{3.21}$$

We use (3.19)-(3.21) to construct the graph structure which is depicted in Fig. 3.3. The joint state variables denoted by $\overline{\mathbf{x}}_k$ needs to be updated within each building

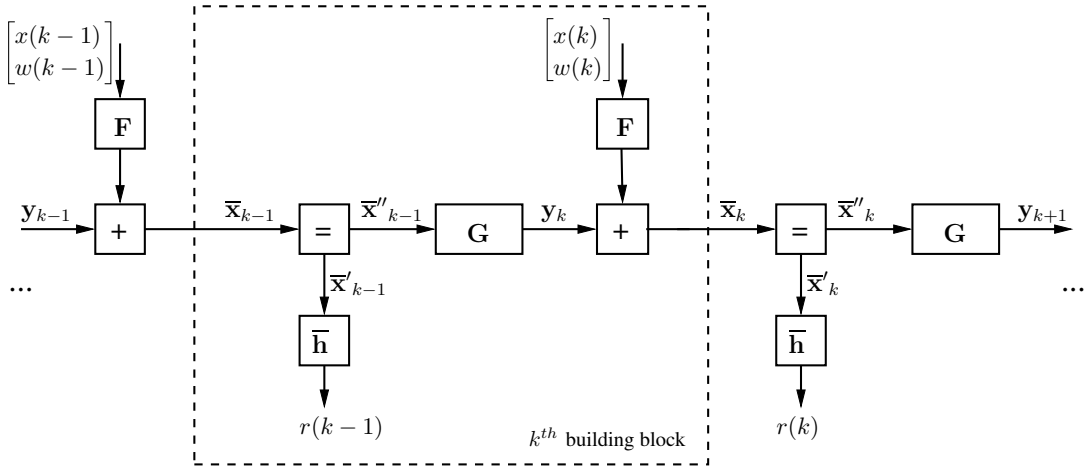

Figure 3.3: Reduced Complexity Factor Graph Structure for LMMSE Filtering under AR Noise Process

block. For the transitions, we define

$$\mathbf{G} = \begin{bmatrix} \mathbf{0}_{J\times 1} & \mathbf{I}_J & \mathbf{0}_{J\times 1} & \mathbf{0}_{J\times(p-1)} \\ 0 & \mathbf{0}_{1\times J} & 0 & \mathbf{0}_{1\times(p-1)} \\ \mathbf{0}_{(p-1)\times 1} & \mathbf{0}_{(p-1)\times J} & \mathbf{0}_{(p-1)\times 1} & \mathbf{I}_{p-1} \\ 0 & \mathbf{0}_{1\times J} & [\text{———}\ \mathbf{a}\ \text{———}] & \end{bmatrix}, \tag{3.22}$$

$$\mathbf{F} = \begin{bmatrix} \mathbf{0}_{J\times 1} & \mathbf{0}_{J\times 1} \\ 1 & 0 \\ \mathbf{0}_{(p-1)\times 1} & \mathbf{0}_{(p-1)\times 1} \\ 0 & 1 \end{bmatrix} \tag{3.23}$$

where $\mathbf{a}$ is defined as the AR parameter vector, i.e., $\mathbf{a} = [a(p)\ a(p-1)\ \ldots\ a(1)]$, $\mathbf{I}_j$ denotes the identity matrix of size $j \times j$, and $\mathbf{0}$ denotes the all zero vector or matrix with the specified sizes. The state variables are updated through the use of $\mathbf{F}$ and $\mathbf{G}$ as follows:

$$\overline{\mathbf{x}}_k = \mathbf{F}\ [x(k) \quad w(k)]^T + \mathbf{y}_k, \text{ where} \tag{3.24}$$

$$\mathbf{y}_k = \mathbf{G}\ \overline{\mathbf{x}}_{k-1}. \tag{3.25}$$

The operations in (3.19)-(3.25) can be followed on the factor graph given in Fig. 3.3.

The message passing algorithm performed on the presented graph is exactly the same as the one mentioned in Chapter 2. The *a posteriori* mean and variance values of the state variables ($\mathbf{m}_{\overline{\mathbf{x}}_k}^{post}$, $\mathbf{V}_{\overline{\mathbf{x}}_k}^{post}$) are obtained by (2.24)-(2.25) using the results of the GMP rules given in Table 2.1-2.2 through forward and backward recursions explained in Chapter 2.

The source signal related part is indeed included in the first L rows of the joint state variable vector $\overline{\mathbf{x}}_k$. Hence, the *a posteriori* mean and variance values of interest are extracted (noise part is stripped out) after performing the calculations given in (2.24)-(2.25). It should be pointed out that the mean value of the state variable $r(k)$ is equal to the k^{th} observation and its variance is equal to 0. This value of 0 causes matrix inversion problems, hence sufficiently small but non-zero number for proper operation should be used. (10^{-5} is chosen judiciously in Matlab simulations). Another important note is that the *a priori* mean and variance values for the input signal at time k ($m_{x(k)}^{prior}$,$v_{x(k)}^{prior}$) are involved in the graph in a way that they are concatenated with the mean and variance values of the zero mean white Gaussian noise $w(k)$ as in (3.24). Since $x(k)$ and $w(k)$ are independent random variables, the total *a priori* information given to the k^{th} building block ($\mathbf{m}_k^{prior}$,$\mathbf{v}_k^{prior}$) can be written as

$$\mathbf{m}_k^{prior} = \begin{bmatrix} m_{x(k)}^{prior} \\ 0 \end{bmatrix}, \tag{3.26}$$

$$\mathbf{v}_k^{prior} = \begin{bmatrix} v_{x(k)}^{prior} & 0 \\ 0 & \sigma_w^2 \end{bmatrix}. \tag{3.27}$$

The source is assumed to generate a white complex Gaussian signal sequence as $x(k) \sim CN(0,1)$, so we can say that $m_{x(k)}^{prior} = 0$ and $v_{x(k)}^{prior} = 1$ in (3.26) and (3.27).

The complexity of this algorithm is also determined similarly to Chapter 2. Main contribution is caused by the matrix inversions in (2.24)-(2.25) resulting in $O((L+p)^3)$ where p is the number of AR parameters of the noise process. However, these operations are to be performed once for every L building blocks owing to the shifting structure of the joint state variable vector $\overline{\mathbf{x}}_k$ over building blocks. Since there are N building blocks, the overall complexity is $O(N(L+p)^3/L)$ which is approximately $O(N(L+p)^2)$ whereas the algorithm proposed for white noise [17] and explained in Chapter 2 has $O(NL^2)$ complexity. We use the performance results of the factor

graph in Chapter 2 which operates under the assumption that the noise is a white random process so as to make a comparison with the presented graph here.

It should be noted that our method provides a computational complexity linearly increasing with N for a non-white Gaussian AR noise process. Besides, it is still possible to use this approach for other non-white noise processes through an approximation as detailed in Section 3.7.

3.5 Theoretical MSE Computation

For the system described in (3.2) and Fig. 3.1, theoretical MSE values are useful to verify the Monte Carlo simulation results to be shown in the next section. Therefore, we will compute the MSE values for both the conventional block LMMSE filter in which the non white statistics of noise process are taken into consideration and the one which operates under white Gaussian noise process assumption. It should be noted that the MSE values obtained here are also corresponds to the MSE values calculated at the first iteration in a coded communication system.

For the matrix representation given in (3.4), the estimated symbol vector after the LMMSE filtering operation can be written as

$$\hat{\mathbf{x}} = \mathbf{W}\,\mathbf{r}. \tag{3.28}$$

In (3.28), $\mathbf{W}$ represents the LMMSE coefficient matrix which is written in default of *a priori* information as [22]

$$\mathbf{W} = \mathbf{C}_{\mathbf{xr}}\,\left(\mathbf{C}_{\mathbf{r}}\right)^{-1}, \tag{3.29}$$

where the covariance matrix $\mathbf{C}_{\mathbf{r}}$ of the observation vector $\mathbf{r}$ and the cross covariance matrix $\mathbf{C}_{\mathbf{xr}}$ of the input vector $\mathbf{x}$ and the observation vector are as follows in consideration of the zero mean noise process and the input signal with $\mathbf{C}_{\mathbf{x}} = \mathbf{I}_{N\times 1}$

$$\mathbf{C}_{\mathbf{r}} = \mathbf{H}\mathbf{H}^{H} + \mathbf{R}_{\mathbf{n}}, \quad \text{and} \tag{3.30}$$

$$\mathbf{C}_{\mathbf{xr}} = \mathbf{H}^{H}; \tag{3.31}$$

and $\mathbf{R}_{\mathbf{n}}$ is given by (3.3) for the AR Gaussian noise process discussed here.

MSE left as the residue from the LMMSE filter which uses the statistics of the colored noise process (MSE_c) will be [22]

$$\begin{aligned} MSE_c =& E\{|\mathbf{W}\,\mathbf{r} - \mathbf{x}|^2\} \\ &= \left(\mathbf{I} + \mathbf{H}^H\,\mathbf{R}_\mathbf{n}^{-1}\,\mathbf{H}\right)^{-1}. \end{aligned} \tag{3.32}$$

On the other hand, LMMSE filter which assumes that the noise is a white Gaussian random process takes the autocorrelation term $\mathbf{R_n}$ in (3.30) as identity matrix $\mathbf{I}$, so the LMMSE coefficient matric under this assumption, $\mathbf{W}_{wa}$, will be

$$\mathbf{W}_{wa} = \mathbf{H}^H\,\left(\mathbf{H}\mathbf{H}^H + \mathbf{I}\right)^{-1}. \tag{3.33}$$

Then, its MSE (MSE_{wa}) can be written as

$$\begin{aligned} MSE_{wa} &= E\{|\mathbf{W}_{wa}\,\mathbf{r} - \mathbf{x}|^2\} \\ &= \mathbf{H}^H\left(\mathbf{I} + \mathbf{H}\mathbf{H}^H\right)^{-1}\left(\mathbf{R_n} + \mathbf{H}\mathbf{H}^H\right)\left(\mathbf{I} + \mathbf{H}\mathbf{H}^H\right)^{-1}\mathbf{H} \\ &\quad - 2\,\mathbf{H}^H\left(\mathbf{I} + \mathbf{H}\mathbf{H}^H\right)^{-1}\mathbf{H} + \mathbf{I}. \end{aligned} \tag{3.34}$$

We use MSE_c and MSE_{wa} to confirm the simulation results of the factor graph structures obtained by Monte Carlo method. Moreover, we will compare MSE_c and MSE_{wa} asymptotically to investigate how the colored statistics of noise process affect performance results.

3.6 Simulation Results

In this section, performance results of the proposed LMMSE filtering method described in Section 3.4 for the system given in (3.2) with the input sequence length of $N = 1000$ are presented in terms of MSE in Fig. 3.4. For comparison, the performance results of the general graph based LMMSE filtering which corresponds to block LMMSE filter (optimal solution for our case) as mentioned in Section 3.3 and LMMSE filtering method [17] described in Chapter 2 under the assumption of a white Gaussian noise process are also given for the same configuration. The simulations are conducted for the noise processes of first order AR ($p = 1$) with parameters $a(1)$=0.9 and $a(1)$=0.98 respectively for a multi-path static channel of $\sqrt{E_s/6}$ [1 2 0 0 0 1].

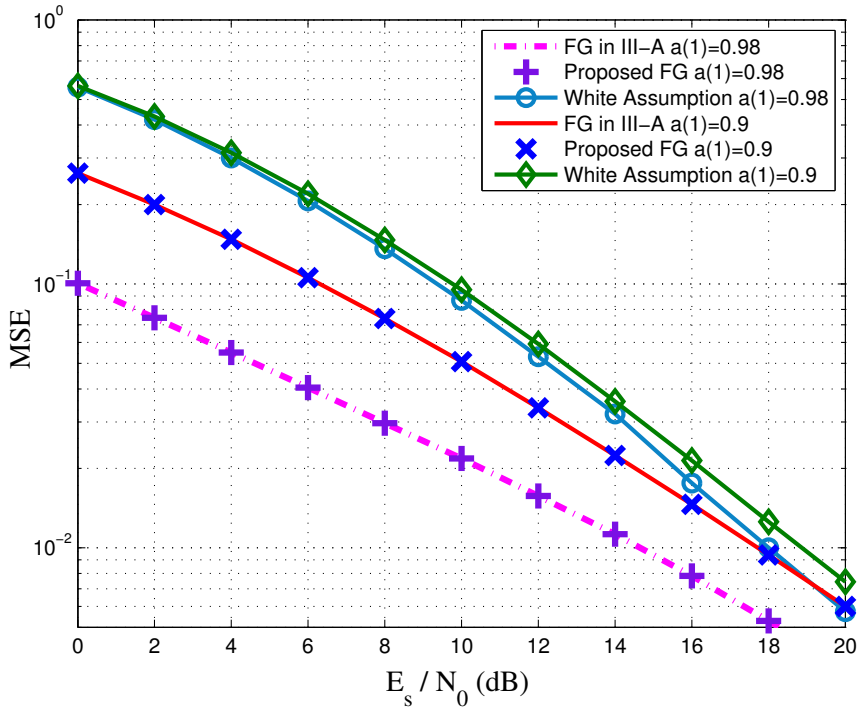

Figure 3.4: Performance of the Proposed Factor Graph Based LMMSE Filter under AR Gaussian Noise Process (Static Channel)

As verified from Fig. 3.4, our proposed method is equivalent to the block LMMSE filter. In addition, it can be seen that the factor graph based LMMSE equalizer in [17] under the white noise assumption performs worse than the methods in which the non-white statistics of the noise process are taken into consideration as expected. Moreover, we observe that the performance of the proposed method improves with increasing $a(1)$ parameter and the improvement compared to the one with white noise assumption also increases because our method uses the correlation information of the noise process which is higher for $a(1)$=0.98. Consequently, although the performance loss of the white noise assumption may be ignored for the lower correlations of the noise process, the proposed factor graph seems to be a good choice with its reduced complexity and higher performance for applications involving high noise correlations in some communication and signal processing problems.

Fig. 3.5 shows the performance results of the same structures under a time varying setting. Simulations are performed for the same configurations as the ones in the static channel scenario except the channel which has independent Rayleigh fading

taps here. The MSE performances averaged over random channel realizations are obtained through the Monte Carlo method. The power delay profile of the channel is also the same as the one in the static channel scenario and the total power of channel taps are normalized, i.e.,

$$E\{|h_j|^2\} = \begin{cases} E_s/6, & j = 1, 6 \\ 2E_s/3, & j = 2 \\ 0 & otherwise \end{cases} . \tag{3.35}$$

As seen from Fig. 3.5, performance results of the proposed structure compared to the ones with white noise assumption (for both $a(1) = 0.98$ and 0.9) are similar to the results in the static channel scenario. Hence, using such a method in which the statistics of non-white noise is taken into consideration will be advantageous in time varying channels as well.

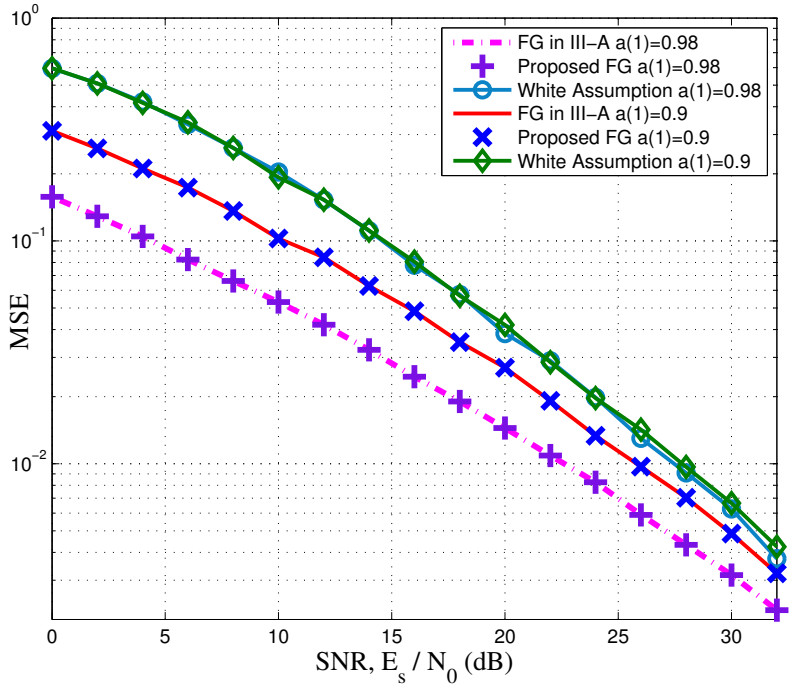

Figure 3.5: Performance of the Proposed Factor Graph Based LMMSE Filter under AR Gaussian Noise Process (Rayleigh Fading Channel)

Finally, we would like to compare those results obtained by the Monte Carlo method in Fig. 3.4 with the theoretical MSE values computed for exactly the same scenario

using (3.32), (3.34) in a wider SNR region to observe the asymptotic behavior of our proposed factor graph and the one with white noise assumption. First of all, the results in Fig. 3.6 and 3.7 confirm our simulation results in Fig. 3.4. Moreover, there are two important results which can be seen from Fig. 3.6 and 3.7. Firstly, LMMSE solution under white noise assumption asymptotically converges to the LMMSE solution which includes the non white statistics of noise process for both $a(1) = 0.9$ and $a(1) = 0.98$ scenarios. The second critical point is that as the noise correlation decreases, the SNR loss which results from ignoring the non white statistics of noise decreases. In other words, LMMSE solution under white noise assumption converges faster for $a(1) = 0.9$ which has a lower correlation than $a(1) = 0.98$. Hence, neglecting the colored characteristics of noise process may not cause degraded performance results all the time. There is a tradeoff between the AR parameter number p which increases the computational complexity and the performance gain it provides to include those p parameters in the factor graph representation. Therefore, the advantages of using the proposed algorithm depend on the application.

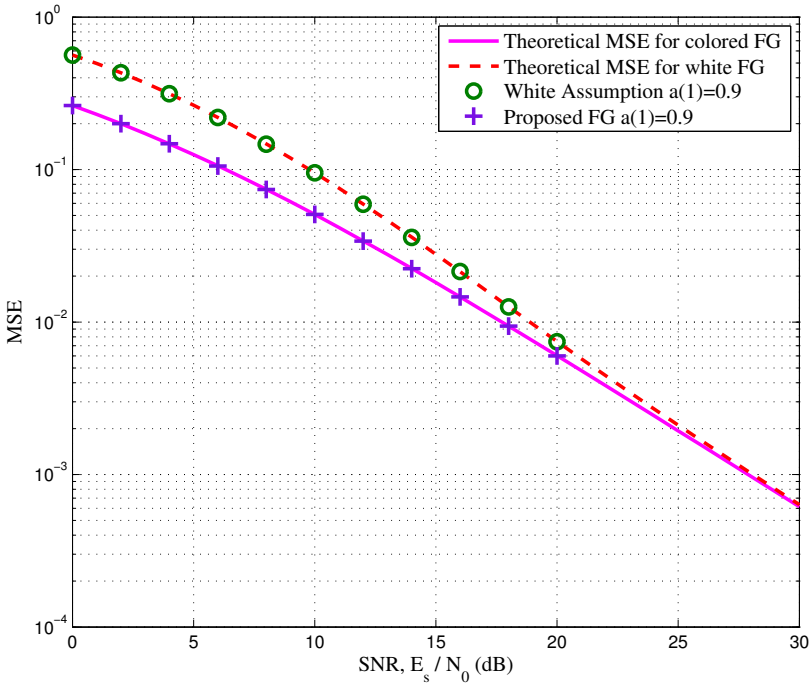

Figure 3.6: Factor Graph Based LMMSE Filter Performances under AR Gaussian Noise Process with a(1)=0.9 as Compared to Theoretical Curves

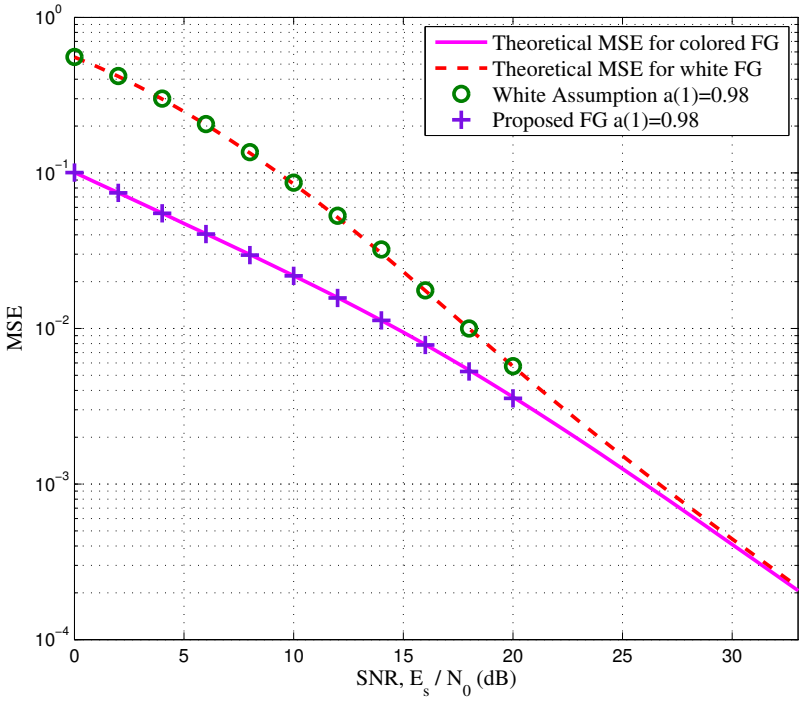

Figure 3.7: Factor Graph Based LMMSE Filter Performances under AR Gaussian Noise Process with a(1)=0.98 as Compared to Theoretical Curves

3.7 Generalization to Other Processes

Although we propose a new graph based LMMSE filter for a specific type of non-white noise process in Section 3.4, it is still possible to use this method for any kind of stationary noise process by means of an approximation. In other words, any wide-sense stationary noise process with known autocorrelation function can be approximated to an AR process by using the Yule-Walker equations [7] given in (3.3).

By choosing a proper value of p and utilizing the first $p+1$ samples of the original autocorrelation function $R_n(j)$ through (3.3), approximate AR process parameters, $a(1), a(2), \ldots, a(p)$, and the variance of the additive white Gaussian noise term in (3.1), σ_w^2, can be obtained as follows. The matrix representation of (3.3) can be written similar to [2] as

$$\mathbf{v} = \mathbf{R}_{nn}\tilde{\mathbf{a}} \quad \text{where} \tag{3.36}$$

$$\mathbf{v} = [R_n(1)\ R_n(2)\ \ldots\ R_n(p)]^T, \tag{3.37}$$

$$\tilde{\mathbf{a}} = [a(1)\ a(2)\ \ldots\ a(p)]^T \quad \text{and} \tag{3.38}$$

$$\mathbf{R}_{nn} = \begin{bmatrix} R_n(0) & R_n(-1) & \dots & R_n(-p+1) \\ R_n(1) & R_n(0) & \dots & R_n(-p+2) \\ \vdots & \vdots & \ddots & \vdots \\ R_n(p-1) & R_n(p-2) & \dots & R_n(0) \end{bmatrix}. \tag{3.39}$$

The AR parameters can be found by using (3.36) as

$$\tilde{\mathbf{a}} = \mathbf{R}_{nn}^{-1}\mathbf{v}. \tag{3.40}$$

With the help of the resultant AR parameters $\tilde{\mathbf{a}}$ from (3.40) and the samples of the original autocorrelation function, σ_w^2 can be computed by

$$\sigma_w^2 = R_n(0) - \sum_{i=1}^{p} a(i) R_n(-i). \tag{3.41}$$

However, the matrix inversion in (3.40) may cause inaccurate results due to ill conditioning of autocorrelation matrix $\mathbf{R}_{nn}$ when the parameter number p is great [2, 20]. This can be seen by the determinant of $\mathbf{R}_{nn}$ which given in [2, 20] as follows

$$|\mathbf{R}_{nn}| = \prod_{m=0}^{p-1} \sigma_m^2, \tag{3.42}$$

where σ_m^2 corresponds to the driving variance of the innovation term when m-order AR process model is used. Hence, the determinant value $|\mathbf{R}_{nn}|$ is getting closer to 0 if the values of σ_m^2 are very small with larger p due to product operation. In other words, $\mathbf{R}_{nn}$ is about to be singular in such a case which may results in unavoidable errors in the matrix inversion in (3.40). To prevent this phenomena, it was proposed to add a small ϵ value to the diagonal entries of $\mathbf{R}_{nn}$, i.e. to $R_n(0)$ [2, 20] so that the ill conditioning of $\mathbf{R}_{nn}$ is tried to be fixed by increasing the ratio of its smallest eigenvalue to the greatest one. The value of ϵ is stated to be chosen judiciously. The presented method here is also used in the example application to be given in the next chapter.

CHAPTER 4

FASTER THAN NYQUIST SIGNALING: AN APPLICATION FOR EQUALIZATION UNDER COLORED NOISE PROCESS

In this section, we present an example application using the proposed method in Chapter 3, FTN signalling, which inherently involves a noise process with non-white statistics. First, we describe the system model for FTN signalling and present the effects of ISI and colored noise on the equivalent model. Then, we show how to adjust our proposed factor graph based LMMSE equalizer depicted in Chapter 3 to cope with both the ISI effect and the non-white statistics of the noise process induced by FTN signaling.

4.1 System Model

FTN signalling is a technique which provides to increase the spectral efficiency by higher transmission rate beyond the Nyquist criterion in the same spectral shape consuming the same energy per bit [1]. In the classical scenario, T-orthogonal pulse shape which prevents ISI after matched filtering operation is used. On the other hand, in FTN signaling, the pulses can be packed by violating the Nyquist rate without decreasing the minimum Euclidean distance (d^2_{min}) in the signaling space [37]. However, there is a limit on the minimum symbol time until which d^2_{min} is not below the value of the case with orthogonal pulse shape. It is called the Mazo limit [36].

Since FTN signaling has more symbols to be packed in the time interval T than the conventional orthogonal signaling, there exists intentional ISI which causes an increase in the receiver complexity. In addition, the sampling rate beyond the Nyquist

criterion at the receiver side brings on colored noise process. To observe those effects mathematically, we present the system model including the whole block diagram of the transmitter and the receiver structures for FTN signaling under AWGN channel in Fig. 4.1. We consider a baseband communication system using complex valued

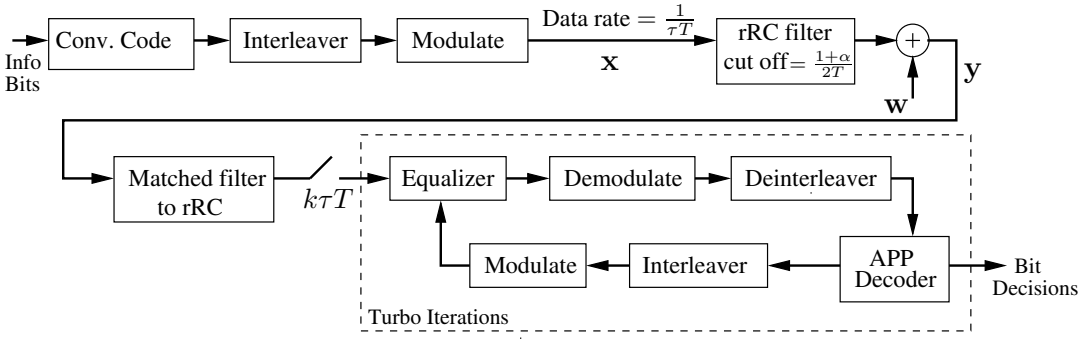

Figure 4.1: System Model

constellations M-QAM from an alphabet S. As given in Fig. 4.1, at the transmitter side, an information symbol x_m which is modulated from b coded information bits is passed through a T-orthogonal root-raised-cosine (rRC) pulse shaping filter $p(t)$, where m is the symbol index. The average symbol energy is E_s, i.e., $E_s = E\{|x_m|^2\}$. The signaling rate is $1/\tau T$; in other words, each symbol is transmitted in a time duration of τT. Here, τ is the packing ratio of symbols which ranges between 0 and 1. If $\tau = 1$, system does not suffer from ISI since the pulse is T-orthogonal. ISI pattern arising from FTN signaling occurs when $\tau < 1$ and as τ decreases, transmission rate increases. The excess bandwidth of rRC filter is denoted by α and we assume $p(t)$ is of unit energy. The received signal under the AWGN channel is written as follows [37]:

$$y(t) = \sum_{m=-\infty}^{\infty} x_m p(t - m\tau T) + w(t), \tau < 1 \tag{4.1}$$

where $w(t)$ represents aditive white zero mean circularly symmetric complex Gaussian noise with average power N_0, i.e., $w(t) \sim CN(0, N_0)$. The signal at the k^{th} discrete time instant at the output of the matched filter after sampling with period of

τT will become

$$r_k = \int_{-\infty}^{\infty} y(t)p^*(t - k\tau T)dt. \tag{4.2}$$

Inserting the expression for $y(t)$ in (4.1) gives

$$r_k = \sum_{m=-\infty}^{\infty} x_m \tilde{h}[m-k] + \tilde{n}_k, \tag{4.3}$$

where

$$\tilde{h}[m-k] = \int_{-\infty}^{\infty} p(t - m\tau T)p^*(t - k\tau T)dt \tag{4.4}$$

and

$$\tilde{n}_k = \int_{-\infty}^{\infty} w(t)p^*(t - k\tau T)dt. \tag{4.5}$$

The autocorrelation of the noise sequence $\tilde{\mathbf{n}}$ is then

$$E\left\{\tilde{n}[m]\tilde{n}^*[k]\right\} = N_0\tilde{h}[m-k]. \tag{4.6}$$

As mentioned above, FTN results in unavoidable ISI and non-white noise samples which in turn worsen the error performance and increase the receiver complexity. What we propose to overcome these issues is a factor graph based LMMSE equalization method in which the non-white noise is taken into consideration while obtaining higher transmission rate with enhanced performance. We use the equalizer structure explained in Chapter 3 through an approximation to AR noise process as given in Section 3.7. Our proposed equalizer can be easily used in an iterative receiver including an APP decoder as given in Fig. 4.1.

4.2 State Space Representation of the Proposed Factor Graph for FTN Signalling

FTN signalling inherently involves both precursor and postcursor ISI as one can deduct from (4.4). We make use of the factor graph structure shown in Fig. 3.3 and explained in Section 3.4. However, we need to modify the joint state variable vector $\overline{\mathbf{x}}_k$ in Section 3.4 so that the postcursor ISI is also included. In the factor graph representation for FTN signalling, it is assumed that the discrete time system model

described by (4.3) can be approximated with $2L+1$ channel taps, i.e., the approximated channel coefficient vector $\mathbf{h}$ is denoted by

$$\mathbf{h} = [h_L \; h_{L-1} \; \ldots \; h_0 \; \ldots \; h_{-L}], \tag{4.7}$$

and the noise process $\tilde{\mathbf{n}}$ is approximated to a Gaussian AR process $\mathbf{n}$ with p parameters as in (3.1), i.e.,

$$n_k = \sum_{i=1}^{p} a_i n_{k-i} + \gamma_k \tag{4.8}$$

where a_i's are AR parameters and γ_k is a white ZMCSCG process with variance σ_γ^2. The approximation to a p-order AR process $\mathbf{n}$ is performed by Yule Walker equations with the diagonal loading operation as detailed in Section 3.7.

Consequently, the k^{th} element of the observation vector $\mathbf{r}$ can be approximated by

$$\begin{aligned} r_k =& \mathbf{h} \; [x_{k-L} \; x_{k-L+1} \; \ldots \; x_k \; \ldots \; x_{k+L}]^T + n_k, && (4.9)\\ =& \overline{\mathbf{h}} \; \overline{\mathbf{x}}_k^T + \gamma_k, \text{ where} && (4.10)\\ \overline{\mathbf{h}} =& [\mathbf{h} \quad 0 \; \ldots \; 0 \; 1]_{(2L+p+1)x1}, && (4.11)\\ \overline{\mathbf{x}}_k =& [x_{k-L} \; \ldots \; x_k \; \ldots \; x_{k+L} \; n_{k-p+1} \; \ldots \; n_k]^T. && (4.12) \end{aligned}$$

Although the extension of the transition matrices $\mathbf{F}$ and $\mathbf{G}$ to this scenario is straightforward, we present these matrices for completeness as below

$$\mathbf{G} = \begin{bmatrix} \mathbf{0}_{2L\times 1} & \mathbf{I}_{2L} & \mathbf{0}_{2L\times 1} & \mathbf{0}_{2L\times(p-1)} \\ 0 & \mathbf{0}_{1\times 2L} & 0 & \mathbf{0}_{1\times(p-1)} \\ \mathbf{0}_{(p-1)\times 1} & \mathbf{0}_{(p-1)\times 2L} & \mathbf{0}_{(p-1)\times 1} & \mathbf{I}_{p-1} \\ 0 & \mathbf{0}_{1\times 2L} & [\text{---------- } \mathbf{a} \text{ ----------}] & \end{bmatrix}, \tag{4.13}$$

$$\mathbf{F} = \begin{bmatrix} \mathbf{0}_{2L\times 1} & \mathbf{0}_{2L\times 1} \\ 1 & 0 \\ \mathbf{0}_{(p-1)\times 1} & \mathbf{0}_{(p-1)\times 1} \\ 0 & 1 \end{bmatrix} \tag{4.14}$$

where $\mathbf{a}$ is defined as the AR parameter vector, i.e., $\mathbf{a} = [a(p) \; a(p-1) \; \ldots \; a(1)]$, $\mathbf{I}_j$ denotes the identity matrix of size $j \times j$, $\mathbf{0}$ denotes the all zero vector or matrix with

the specified sizes. The update of the state variables occurs through the use of $\mathbf{F}$ and $\mathbf{G}$ as follows:

$$\overline{\mathbf{x}}_k = \mathbf{F} \begin{bmatrix} x_{k+L} & \gamma_k \end{bmatrix}^T + \mathbf{y}_k, \text{ where} \tag{4.15}$$

$$\mathbf{y}_k = \mathbf{G}\, \overline{\mathbf{x}}_{k-1}. \tag{4.16}$$

Overall, we construct the graph based equalizer structure for FTN signaling on the basis of the idea presented in Chapter 3 by using the state space representation described in (4.9)-(4.16). Since the graph structure and the GMP algorithms to be applied on this graph are provided in Chapter 3, we do not repeat these details here. The only difference here is in the state variable vector $\overline{\mathbf{x}}_k$ and consequently in the state space model which are reorganized in (4.9)-(4.16) in a way to include the postcursor ISI. For the transitions between our graph based equalizer (Gaussian domain) and the APP decoder (binary, i.e., bit LLR domain), we use the LLR exchange algorithms explained in Section 2.2.3.

In FTN signalling, we utilize two approximations so that our proposed graph based solution is not equivalent to LMMSE filtering:

- Assumption of a finite length ISI channel and
- Approximation to Gaussian AR noise process.

However, the presented approach still provides good performance results and is an attractive alternative particularly for higher order modulation alphabets owing to its reduced complexity. On the other hand, it should be noted that the graph based LMMSE [17] described in Chapter 2 under white noise assumption may perform very close to the proposed approach in this section when the correlation of the noise process is very low. Depending on the noise correlation and the number of the AR parameters used for the approximation on the graph in Fig. 3.3, it should be determined whether it is advantageous or not to take the noise statistics into account.

4.3 Complexity Comparison to Other Studies in the Literature

In FTN signaling, trellis based algorithms such as the Viterbi algorithm [33] and BCJR [3] are frequently used in the literature due to the existence of ISI. However, the trellis becomes extremely large when there is a large channel delay spread caused by small τ in equivalent model and/or whenever a high-order constellation is utilized. There are recently proposed reduced complexity algorithms in [39] and [32]. In [32], $\mathcal{M}$-BCJR algorithm based on searching only a subset of the whole trellis is analyzed. Its approximate complexity is $O(\mathcal{M}N)$ with the additional complexity due to the use of a whitening filter, where $\mathcal{M}$ is the number of trellis states visited for each symbol. The required $\mathcal{M}$ value for a sensible BER performance usually increases exponentially with constellation size M and number of ISI taps. Moreover, there needs to be an optimization of the whitening filter for the $\mathcal{M}$-BCJR algorithm as mentioned in [32] which may lead to a problem for time selective fading environments with this challenging optimization requirement. In [39], a frequency domain MMSE equalization method with a complexity of $O\left(N\log(N)\right)$ is proposed for uncoded FTN systems without any adaptation to coding schemes. Because of the absence of a coding scheme and a turbo iterative structure using soft information of bits, it is observed that there is 3-5 dB performance loss in BER performance even above the Mazo limit (higher τ than τ^*). In addition, frequency domain MMSE equalization causes a decrease in efficiency due to the cyclic prefix. Furthermore, one should remember that the previously studied graph given in Section 3.3 may not be the first choice either due to its complexity of $O(N^3)$. However, it can still serve as a means to put a lower bound on our proposed reduced complexity graph approach since it uses the noise statistics directly without any approximations.

On the other hand, the complexity of the presented graph approach in Section 4.2 is $O(N\mathcal{L}^2)$ where $\mathcal{L}$ is the sum of the number of ISI taps and the parameter number (p) used in the approximation of the noise process to an AR process, i.e., $\mathcal{L} = 2L + p + 1$ using the result of Section 3.4. It should be noted that $\mathcal{L}$ does not change with the constellation size and scales up only linearly with the ISI length. Moreover, this graph approach can easily be adapted to the time selective fading environments by modifying the channel taps in the building blocks.

4.4 Simulation Results

In this section, we present our performance results of FTN signaling in terms of bit error rate (BER) for different scenarios. In all schemes, a convolutional code with code rate $1/2$ and generator polynomial $(7, 5)$ is used and we assume that a rRC filter with $\alpha = 0.3$ and time delay of $8T$ is implemented. To make a comparison, we also provide the performance results of the same convolutionally coded system using the conventional orthogonal transmission over the AWGN channel for which the receiver explained in Section 2.3 by (2.53)-(2.54) is operated. It is called as "AWGN" in Fig. 4.2-4.7.

First we start with BPSK signalling. The Mazo limit under the described scenario for BPSK signalling is $1/3$ [36] where the simulation results for $\tau = 0.5$ are presented in Fig. 4.2-4.3. This means two times higher spectral efficiency as compared to no FTN signalling case, i.e., $\tau = 1$. In the simulation settings, uncoded 1000 bits are transmitted over AWGN channel. With the given α and the time delay values, $\tau = 0.5$ results in 65 inherent ISI taps which is truncated to 15 taps in the the approximated system model given in (4.7), i.e., $L = 7$ for the reduced graph based LMMSE equalizer described in Section 4.2. The approximation of the noise to an AR process is performed according to (4.6) with 5 parameters, i.e., $p = 5$. For the diagonal loading mentioned in Section 3.7, $\epsilon = 10^{-2}$ value is chosen judiciously. The number of turbo iterations is 5 and the scaling factors δ, ρ which are multiplied by the LLR values at the equalizer and decoder output respectively are chosen by trial and error and specified in Fig. 4.2-4.3. Similar scaling operations are also encountered in many iterative receiver structures in the literature which prevents overconfident messages and improves the performance of the receiver [9, 14, 19, 32]. The performance results of this proposed structure with respect to iterations is shown in Fig. 4.2. As verified from Fig. 4.2, 4 or 5 iterations are enough to obtain a performance close to the no FTN signalling case which is referred to AWGN.

Fig. 4.3 shows the comparative results of alternative equalizer structures for the same τ value. The general graph based LMMSE equalizer described in Section 3.3 is presented as a lower bound to our method since it does not truncate the ISI channel vector and uses the statistics of noise process directly without any approximation. It is op-

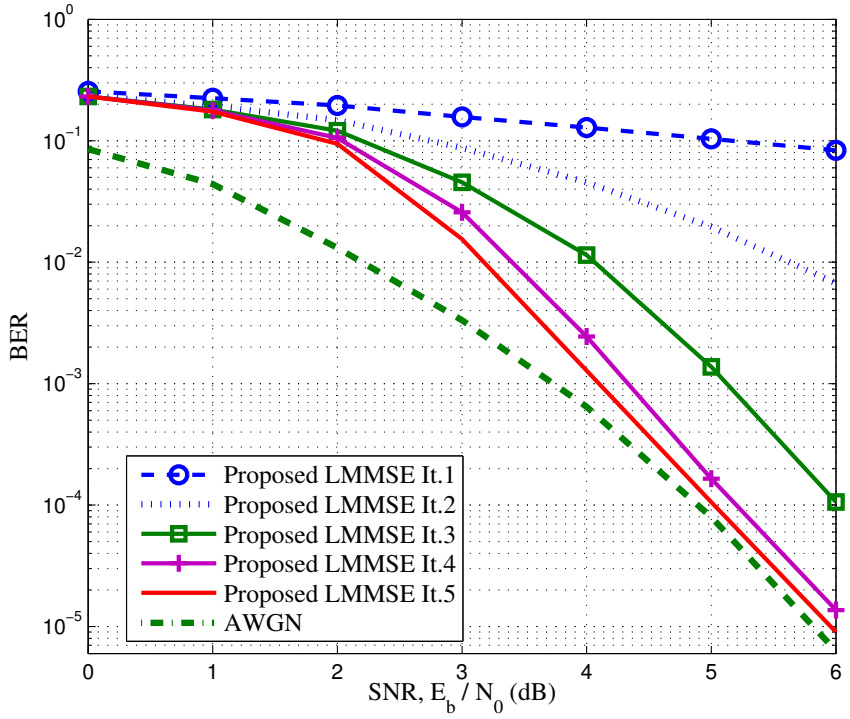

Figure 4.2: Performance Results of the Proposed Graph Based LMMSE Equalizer for FTN signaling with $\tau = 0.5$ ($\delta = 1$, $\rho = 0.67$) - BPSK Signalling

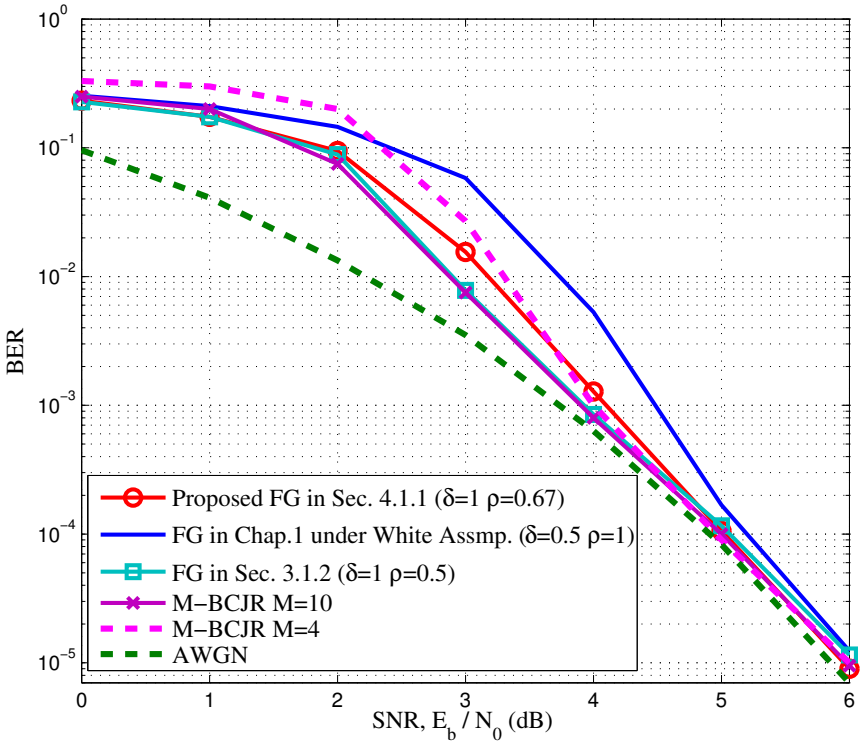

Figure 4.3: Comparative Performance Results of Receiver Structures for FTN Signaling with $\tau = 0.5$ - BPSK Signalling

erated by sending 750 uncoded bits due to its high complexity. In addition, we also present the performance results of the graph detailed in Chapter 2 under white noise assumption which is also operated with the truncated 15-tap channel. For these two LMMSE equalizer structures, the number of turbo iterations is also 5 and the chosen scaling factors δ, ρ are also specified in Fig. 4.3.

In addition, the performance of the $\mathcal{M}$-BCJR algorithm in [32] for the same scenario under BPSK signaling for $\mathcal{M} = 4$ and $\mathcal{M} = 10$ is presented except that $\mathcal{M}$-BCJR in [32] is operated under 6000 uncoded bits and 20 iterations. It is seen from Fig. 4.3 that both the $\mathcal{M}$-BCJR with $\mathcal{M} = 10$ and the proposed graph based equalizer in which the noise statistics are taken into consideration performs very close to no ISI case below BER value of 10^{-3}. On the other hand, the graph detailed in Chapter 2 under white noise assumption has close performance to others such that 0.5 dB SNR loss disappears below the BER value of 10^{-4} since the noise correlation for $\tau = 0.5$ is small.

To promote the proposed method, we present a scenario which includes higher noise correlation in order to see the difference between the performance of our proposed graph and the one operated under a white noise assumption. Fig. 4.4 shows the results for $\tau = 0.4$ which results in 81 ISI taps that are truncated to 19 taps in graph implementation. 3000 uncoded bits are transmitted and 9 iterations are performed for both equalizers. For the proposed method, AR noise approximation method is run with $p = 5$ and $\epsilon = 10^{-2}$ values. As seen from Fig. 4.4, our method has 1 dB SNR gain compared to the graph with white noise assumption at BER value of 10^{-4}. It is expected to see an increase in the difference between those two as the τ value decreases due to higher noise correlation. However, the performance of the LMMSE equalizer is observed to deteriorate for smaller τ values since it is a sub-optimal receiver which degrades under severe ISI channels as mentioned in [17]. This can also be realized from the convergence rates of the proposed method to AWGN curve for $\tau = 0.5$ and 0.4 in Fig.s 4.3-4.4. As the ISI severity increases, it approaches to AWGN performance later.

To observe the effect of the number of parameters used in the AR process approximation explained in Section 3.7, we compare the performance results of our proposed

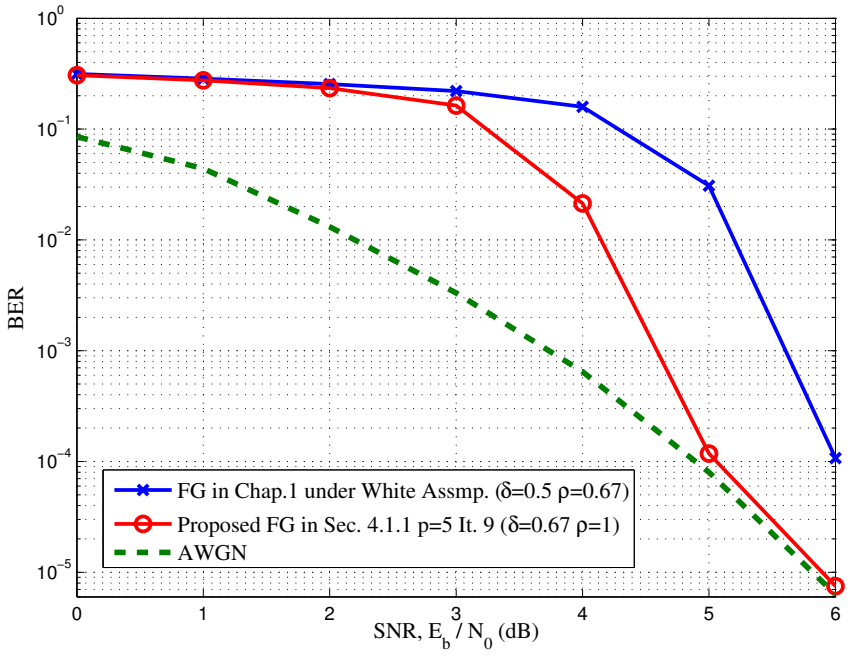

Figure 4.4: Comparative Performance Results of Reduced Graph Based LMMSE Equalizers for FTN Signaling with $\tau = 0.4$ - BPSK Signalling

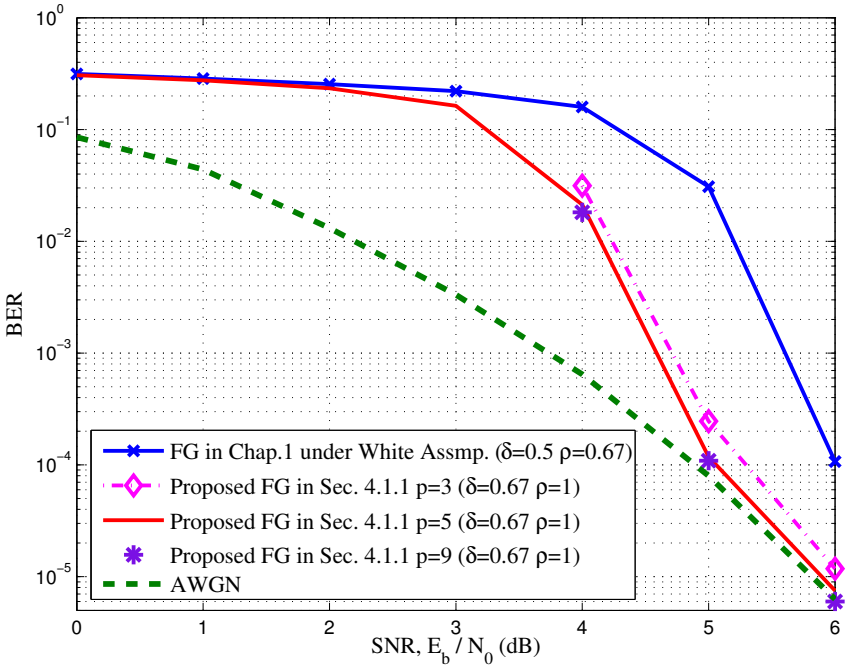

Figure 4.5: Effects of the Number of AR Parameters Used in the Approximation on the Performance Results of Reduced Graph Based LMMSE Equalizers for FTN Signaling with $\tau = 0.4$ - BPSK Signalling

graph structure under the same scenario as the one in Fig. 4.4 except AR parameter number p which is used in the modelling of the noise process and involved in our state space model as given in (4.12). As shown in Fig. 4.5, increasing the number of AR parameters improves BER performance since it provides better approximation to the original autocorrelation function. However, there is no significant benefit to choose greater number for p after some point. For example, $p = 5$ performs almost the same as $p = 9$ in terms of BER. On the other hand, greater p value costs higher computational complexity as detailed in Section 4.3. Hence, p should be chosen small enough to provide the desired performance. Through simulations, we have chosen $p = 5$ by trial and error because we have observed that it resulted in better BER performance than $p < 5$ values. On the other hand, scenarios for $p > 5$ do not provide any critical advantage since the samples of the autocorrelation function corresponding to larger p values are getting smaller.

Finally, we would like to consider higher constellation sizes for which LMMSE equalization has complexity advantage over trellis based methods such as $\mathcal{M}$-BCJR. It should be noted that there is no performance characterization of the proposed methods in the literature for FTN Signaling under high order constellations within the knowledge of the authors. One reason may be the exponentially increasing computational complexity of those methods with the constellation size. For M-QAM signalling simulations here, we use both of our proposed Wang Poor based extrinsic LLR computation methods (exact and approximated versions) explained in Section 2.2.3. The simulations are conducted for Gray encoded 16-QAM signaling under $\tau = 0.67$ which results in a 61-tap ISI channel. The Mazo limit for this case is an open research problem to the best of our knowledge. Our proposed graph structure uses the truncated channel coefficient vector including 11 taps and AR process approximation is made with $p = 5$ and $\epsilon = 0.05$ values. Uncoded 4000 bits are transmitted.

For this setting, Fig. 4.6 shows the comparative performance results of our LMMSE equalizer and the one operated under white noise assumption which both use the exact Wang Poor based LLR exchange algorithm given by (2.37) using 5 turbo iteration. It should be noted that there is no need to use scaling factors to improve the performance when the exact Wang Poor algorithm given in (2.37) is implemented. As seen from Fig. 4.7, the BER performance of the proposed structure is getting closer to no ISI

case particularly below BER of 10^{-3} and has 0.5 dB SNR gain compared to the graph operated under white noise assumption upto BER value of 10^{-4}. This is not a great SNR gain since the noise correlation here is small due to the use of large τ value. It is also interesting to observe that the 16-QAM FTN signaling case with these settings has the same PSD shape and transmission rate as $(7, 5)$ coded ordinary 64-QAM modulation with the same pulse shape filter. However, the performance of the FTN signaling with the proposed graph based LMMSE method has 4 dB SNR advantage with respect to the $(7, 5)$ coded 64-QAM modulation with no FTN below BER of 10^{-3}.

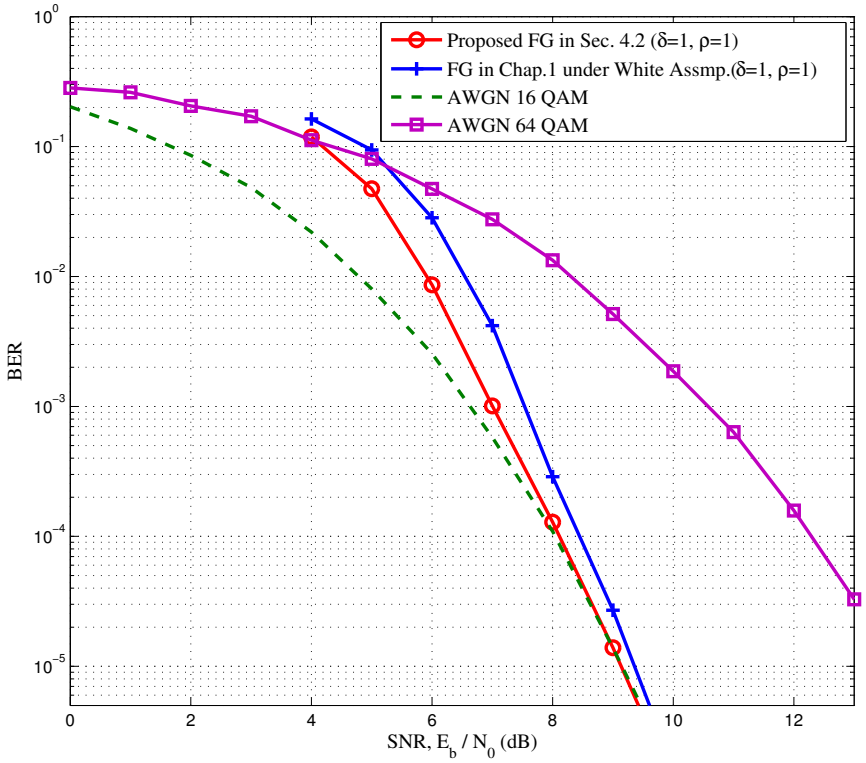

Figure 4.6: Comparative Performance Results of Reduced Graph Based LMMSE Equalizers for FTN Signaling with $\tau = 0.67$ - 16-QAM Signalling (Exact WP Based LLR Computation). Note: Spectral efficiencies are the same.

For the same setting, Fig. 4.7 presents the results for the approximated version of the Wang Poor based LLR exchange algorithm given by (2.39) using 7 turbo iterations. We have observed that similar performances as in Fig. 4.6 can be obtained by applying scaling operations to the LLR output values which improves the BER performance.

This approximated version provides a small decrease in computational complexity per turbo iteration. However, it will be more practical to use the exact one since it eliminates the necessity of finding the best scaling factors by trial and error for each different configuration and the approximated version needs a few more turbo iterations to reach the same performance for this scenario.

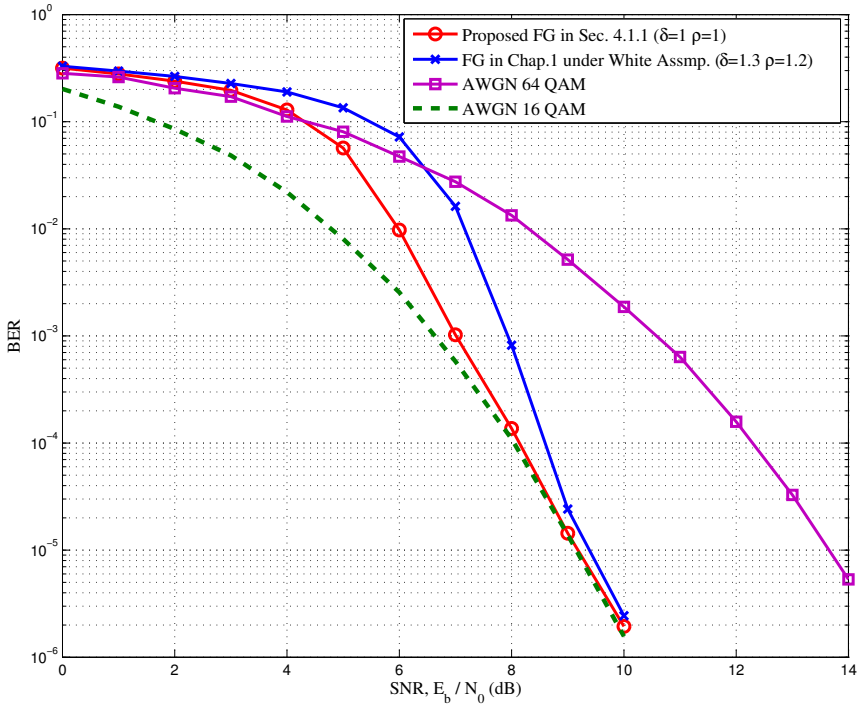

Figure 4.7: Comparative Performance Results of Reduced Graph Based LMMSE Equalizers for FTN Signaling with $\tau = 0.67$ - 16-QAM Signalling (Approximated WP Based LLR Computation). Note: Spectral efficiencies are the same.

4.5 Discussion

In this section, we present an example application including non-white noise process for which we propose the reduced complexity factor graph based LMMSE equalizer. One important point is that any colored random process should be approximated to an AR process with p parameters to be appropriate for the state space representation of the graph as explained in Chapter 3. As explained in Section 4.4, increasing p provides better performance results upto a point. It is observed that there is no significant

benefit to use much more parameters in approximation. Besides, adding more AR parameters to the joint state variable vector in the state space representation causes an increase in complexity.

Therefore, the proposed method here will be attractive for applications which require less parameters for approximation to AR process and involve higher correlation. In such cases, greater SNR gains as compared to the LMMSE equalizer performed under white noise assumption could be obtained by a small increase in complexity. On the other hand, in reverse situations, performing under white process assumption may be reasonable. Hence, it should be determined depending on the application whether the noise statistics are taken into consideration or not.

Regarding FTN Signalling, it may be a beneficial alternative to increase spectral efficiency for some communication systems where high data rates are required. However, it is mentioned in the studies in the literature and also observed through our study that reaching high rates even near the Mazo limit results in severe ISI which costs more complex receiver structures.

CHAPTER 5

FACTOR GRAPH BASED LMMSE EQUALIZER FOR MIMO ISI CHANNELS

In this chapter, we modify the factor graph based equalizer for SISO ISI channels mentioned in Chapter 2 to MIMO ISI systems under white Gaussian noise so as to provide a reduced complexity time domain equalizer alternative to be run in fast fading channels. After defining the system model for MIMO ISI channel scenario, we present the state space structure of the enhanced factor graph together with its complexity analysis. Finally, performance results of the proposed algorithm will be provided as compared to a genie-aided matched filter bound.

5.1 System Model

We consider a MIMO single-carrier communication system which suffers from the ISI effect due to the wireless nature of the channel. The block diagram of the discussed transmitter and receiver structures are given in Fig. 5.1. At the transmitter side, after the coded information bits are interleaved and modulated according to an M-QAM alphabet S, modulated symbols are split to N_t transmit antennas and sent over the ISI channel which occurs between each transmit and receive antenna. At the receiver side, a turbo structure including the proposed graph based LMMSE equalizer and APP decoder is operated by use of observations coming from N_r receive antennas.

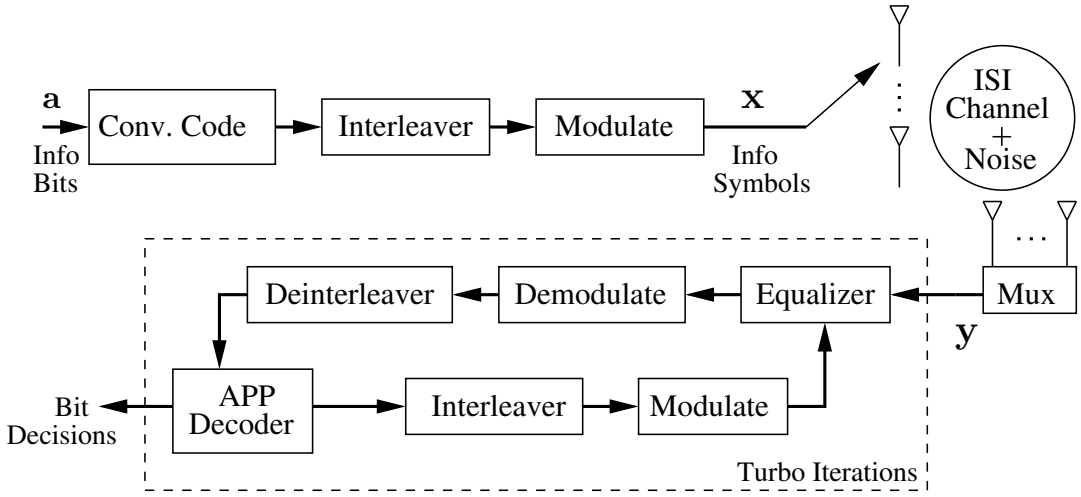

Figure 5.1: System Model

We can model the given discrete-time system at time k as

$$\mathbf{y}_k = \sum_{i=0}^{L-1} \mathbf{H}_i \mathbf{x}_{k-i} + \mathbf{n}_k\,; \quad k = 1, 2, \ldots, N + L - 1, \tag{5.1}$$

$$\mathbf{H}_i = \begin{bmatrix} h_{11}(i) & h_{12}(i) & \ldots & h_{1N_t}(i) \\ h_{21}(i) & h_{22}(i) & \ldots & h_{2N_t}(i) \\ \vdots & \vdots & \vdots & \vdots \\ h_{N_r1}(i) & h_{N_r2}(i) & \ldots & h_{N_rN_t}(i) \end{bmatrix}_{N_r \times N_t} ; \tag{5.2}$$

where L is the number of channel taps; N is the transmission block length; $\mathbf{H}_i$ is the $N_r \times N_t$ channel matrix at time i; $\mathbf{x}_k$ is the transmitted symbol vector of size N_t at time k; $\mathbf{y}_k$ is the observation vector of size N_r at time k and $\mathbf{n}_k$ represents additive white circularly symmetric complex Gaussian noise vector with zero mean and covariance $N_0\mathbf{I}_{N_r}$ at time k, i.e., $\mathbf{n}_k \sim CN(0, N_0\mathbf{I}_{N_r})$. The input symbol sequence is assumed to include independent, identically distributed (i.i.d.) random variables and the transmitted symbol vector $\mathbf{x}_k$ at time k is

$$\mathbf{x}_k = [x_{k,1}\ x_{k,2}\ \ldots\ x_{k,N_t}]^T \quad k = 1, 2, \ldots N \tag{5.3}$$

where $x_{k,l}$ is the symbol transmitted at the l^{th} transmit antenna at time k and its average energy is defined as E_s, i.e., $E\{|x_{k,l}|^2\} \triangleq E_s$. For notational convenience, we define $J \triangleq L - 1$ which denotes the memory of the channel.

The matrix representation of (5.1) could be written as below by combining all observations

$$\mathbf{y} = \mathbf{H}\mathbf{x} + \mathbf{n}, \quad \text{where} \tag{5.4}$$

$$\mathbf{y} = \begin{bmatrix} \mathbf{y}_1 \\ \mathbf{y}_2 \\ \vdots \\ \mathbf{y}_{N+J} \end{bmatrix}_{N_r(N+J)\times 1}, \mathbf{n} = \begin{bmatrix} \mathbf{n}_1 \\ \mathbf{n}_2 \\ \vdots \\ \mathbf{n}_{N+J} \end{bmatrix}_{N_r(N+J)\times 1}, \tag{5.5}$$

$$\mathbf{H} = \begin{bmatrix} \mathbf{H}_0 & \mathbf{0} & \dots & \dots & \dots & \mathbf{0} \\ \mathbf{H}_1 & \mathbf{H}_0 & \ddots & & & \vdots \\ \vdots & & \ddots & \ddots & & \vdots \\ \mathbf{H}_J & \dots & & \mathbf{H}_0 & \ddots & \vdots \\ \mathbf{0} & \ddots & & & \ddots & \mathbf{0} \\ \vdots & \ddots & & \mathbf{H}_J & \dots & \mathbf{H}_0 \\ \vdots & & & \ddots & \ddots & \vdots \\ \mathbf{0} & \dots & \dots & \dots & \mathbf{0} & \mathbf{H}_J \end{bmatrix}_{N_r(N+J)\times N_t N}, \mathbf{x} = \begin{bmatrix} \mathbf{x}_1 \\ \mathbf{x}_2 \\ \vdots \\ \mathbf{x}_N \end{bmatrix}_{N_t N\times 1}. \tag{5.6}$$

For the described system model, the details of the proposed equalizer structure are presented in the subsequent section.

5.2 LMMSE Filtering Based on Reduced Complexity Factor Graph Enhanced for MIMO ISI Systems

For the system described in Fig. 5.1, the observation vector at time k given in (5.1) can be rewritten as

$$\mathbf{y}_k = \overline{\mathbf{H}}\,\overline{\mathbf{x}}_k + \mathbf{n}_k\,; \quad k = 1, 2, \dots, N+J \tag{5.7}$$

where

$$\overline{\mathbf{H}} = [\mathbf{H}_J \quad \mathbf{H}_{J-1} \quad \dots \quad \mathbf{H}_0], \quad \text{and} \tag{5.8}$$

$$\overline{\mathbf{x}}_k = \begin{bmatrix} \mathbf{x}_{k-J} \\ \mathbf{x}_{k-J+1} \\ \vdots \\ \mathbf{x}_k \end{bmatrix}_{N_t L \times 1} . \tag{5.9}$$

We use (5.7)-(5.9) to construct the state space graph representation of the MIMO ISI channels similar to the SISO ISI channel [17] which is detailed in Chapter 2. For transition to the next time instant, $k+1$, we define

$$\mathbf{G} = \begin{bmatrix} \mathbf{0}_{N_t J \times N_t} & \mathbf{I}_{N_t J} \\ \mathbf{0}_{N_t \times N_t} & \mathbf{0}_{N_t \times N_t J} \end{bmatrix}_{N_t L \times N_t L} , \tag{5.10}$$

$$\mathbf{F} = \begin{bmatrix} \mathbf{0}_{N_t J \times N_t} \\ \mathbf{I}_{N_t} \end{bmatrix}_{N_t L \times N_t} \tag{5.11}$$

where $\mathbf{0}$ denotes the all zero matrix of the specified size and $\mathbf{I}_j$ denotes the identity matrix of size j. It can be seen that

$$\overline{\mathbf{x}}_{k+1} = \mathbf{F}\ \mathbf{x}_{k+1} + \mathbf{z}_{k+1}, \quad \text{where} \tag{5.12}$$

$$\mathbf{z}_{k+1} = \mathbf{G}\ \overline{\mathbf{x}}_k \tag{5.13}$$

$$= \begin{bmatrix} \mathbf{x}_{k-J+1} \\ \mathbf{x}_{k-J+2} \\ \vdots \\ \mathbf{x}_k \\ \mathbf{0}_{N_t \times 1} \end{bmatrix} .$$

The factor graph representation corresponding to (5.7)-(5.13) can be seen in Fig. 5.2. The message passing algorithm performed on the presented graph is exactly the same as the one mentioned in Chapter 2. Hence, we just refer to the equations and tables instead of repeating them. The *a posteriori* mean and variance values of the state variables $(\mathbf{m}_{\overline{\mathbf{x}}_k}^{post}, \mathbf{V}_{\overline{\mathbf{x}}_k}^{post})$ are obtained by (2.24)-(2.25) using the results of the GMP rules given in Table 2.1-2.2 through forward and backward recursions explained in Chapter 2.

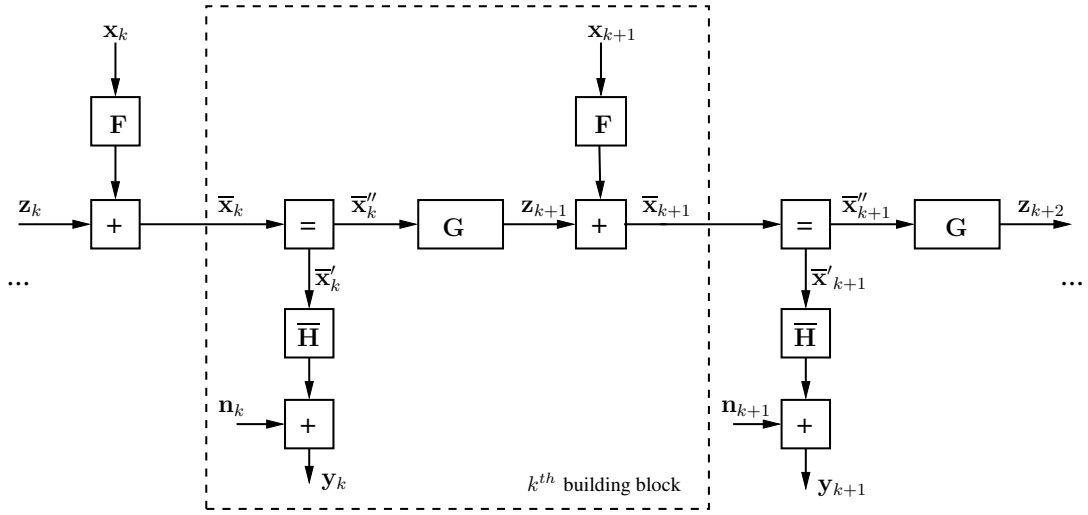

Figure 5.2: Factor Graph of MIMO ISI Channel

The diagonal elements of $\mathbf{V}_{\overline{\mathbf{x}}_k}^{post}$ indicate the *a posteriori* variance values of the symbols sent from all transmit antennas between the time instants $k-J$ and k as given by

$$\mathbf{V}_{\overline{\mathbf{x}}_k}^{post} = \begin{bmatrix} \mathbf{V}_{\mathbf{x}_{k-J}}^{post} & \dots & \dots \\ \dots & \mathbf{V}_{\mathbf{x}_{k-J+1}}^{post} & \dots \\ \dots & \ddots & \dots \\ \dots & \dots & \mathbf{V}_{\mathbf{x}_k}^{post} \end{bmatrix}, \quad \text{where} \tag{5.14}$$

$$diag\{\mathbf{V}_{\overline{\mathbf{x}}_k}^{post}\} = [diag\{\mathbf{V}_{\mathbf{x}_{k-J}}^{post}\} \quad diag\{\mathbf{V}_{\mathbf{x}_{k-J+1}}^{post}\} \ \dots \ diag\{\mathbf{V}_{\mathbf{x}_k}^{post}\}], \tag{5.15}$$

$$diag\{\mathbf{V}_{\mathbf{x}_k}^{post}\} = [v_{x_{k,1}}^{post} \ v_{x_{k,2}}^{post} \ \dots \ v_{x_{k,N_t}}^{post}]. \tag{5.16}$$

In a similar way, the elements of $\mathbf{m}_{\overline{\mathbf{x}}_k}^{post}$ includes the *a posteriori* mean values of the state vector $\overline{\mathbf{x}}_k$ as

$$\mathbf{m}_{\overline{\mathbf{x}}_k}^{post} = \begin{bmatrix} \mathbf{m}_{\mathbf{x}_{k-J}}^{post} \\ \mathbf{m}_{\mathbf{x}_{k-J+1}}^{post} \\ \vdots \\ \mathbf{m}_{\mathbf{x}_k}^{post} \end{bmatrix}, \text{where} \quad \mathbf{m}_{\mathbf{x}_k}^{post} = \begin{bmatrix} m_{x_{k,1}}^{post} \\ m_{x_{k,2}}^{post} \\ \vdots \\ m_{x_{k,N_t}}^{post} \end{bmatrix}. \tag{5.17}$$

Since the elements of the state vector $\overline{\mathbf{x}}_k$ is shifted by N_t symbols through the way to $\overline{\mathbf{x}}_{k+1}$, this shift is also seen at the output mean vectors and variance matrices as

$$\mathbf{V}_{\overline{\mathbf{x}}_{k+1}}^{post} = \begin{bmatrix} \mathbf{V}_{\mathbf{x}_{k-J+1}}^{post} & \dots & \dots \\ \dots & \mathbf{V}_{\mathbf{x}_{k-J+2}}^{post} & \dots \\ \dots & \ddots & \dots \\ \dots & \dots & \mathbf{V}_{\mathbf{x}_{k+1}}^{post} \end{bmatrix}, \; \mathbf{m}_{\overline{\mathbf{x}}_{k+1}}^{post} = \begin{bmatrix} \mathbf{m}_{\mathbf{x}_{k-J+1}}^{post} \\ \mathbf{m}_{\mathbf{x}_{k-J+2}}^{post} \\ \vdots \\ \mathbf{m}_{\mathbf{x}_{k+1}}^{post} \end{bmatrix}. \tag{5.18}$$

It should be noted that the symbols sent from different transmit antennas are assumed to be independent. So, the *a priori* information related to $\mathbf{x}_k$ is involved in the factor graph as

$$\mathbf{m}_{\mathbf{x}_k}^{\downarrow} \triangleq \mathbf{m}_{\mathbf{x}_k}^{prio} = \begin{bmatrix} m_{x_{k,1}}^{prio} \, m_{x_{k,2}}^{prio} \, \dots \, m_{x_{k,N_t}}^{prio} \end{bmatrix}^T, \tag{5.19}$$

$$\mathbf{V}_{\mathbf{x}_k}^{\downarrow} \triangleq \mathbf{V}_{\mathbf{x}_k}^{prio} = \begin{bmatrix} v_{x_{k,1}}^{prio} & 0 & \dots & 0 \\ 0 & v_{x_{k,2}}^{prio} & \ddots & \vdots \\ \vdots & \ddots & \ddots & 0 \\ 0 & \dots & 0 & v_{x_{k,N_t}}^{prio} \end{bmatrix}, \tag{5.20}$$

where $m_{x_{k,l}}^{prio}$ and $v_{x_{k,l}}^{prio}$ are the *a priori* mean and variance values of the symbol transmitted at the k^{th} time instant from the l^{th} transmit antenna. The transitions between the Gaussian and binary bit LLR domains are provided through a straightforward extension of the algorithms detailed in Section 2.2.3 to MIMO systems.

For the complexity analysis, we need to refer to the GMP rules explained in Chapter 2 once more since they are used in exactly the same way on the enlarged graph structure for the equalization of MIMO ISI channels. The major contribution to the complexity of the proposed equalizer structure is due to the matrix inversions in (2.24-2.25), (2.20) and (2.23). In each building block, (2.20) and (2.23) need to be calculated in a complexity of $O(N_r^3)$ since they involve matrix inversions of size N_r thanks to the applied matrix inversion lemma. On the other hand, (2.24) and (2.25) are applied only once for every L building blocks with a complexity of $O(N_t^3 L^3)$ owing to the shifting property of the state vectors as explained in (5.18). Hence, it corresponds to $O(N_t^3 L^2)$ for each building block, i.e., each time instant, while there are

N building blocks in our system. Therefore, the overall complexity is approximately $O(N \cdot max\{N_r^3, N_t^3 L^2\})$ which is equal to $O(N \cdot N_t^3 L^2)$ in most of the cases. As a result of this discussion, the overall complexity per symbol per transmit antenna is about $O(N_t^2 L^2)$ which is reasonably lower than both the block LMMSE filtering operation with a complexity $O(N^2 N_t^2)$ and the other time domain equalizer structures among which the least complex one has $O(N_t^2 L^3)$ complexity as mentioned in Section 1.

5.3 Simulation Results

We conduct our simulations under a quasi-static Rayleigh fading channel scenario with independent ISI taps, i.e., each tap is constant over one block and change independently from block to block. This model is also referred to as the block fading model. The ISI channel between each transmit-receive antenna pair has identical, equal power delay profile, i.e., all L taps have equal energy as given by

$$E\{|h_{ij}(k)|^2\} = 1/L \tag{5.21}$$

where $h_{ij}(k)$ is the k^{th} channel tap between the j^{th} transmit antenna and i^{th} receive antenna. The simulations are based on the system model in Fig. 5.1 with a random interleaver and a rate $1/2$ convolution code whose generator matrix is $(7, 5)_8$ under the modulation types of BPSK, 4-PSK and 16-QAM. In all simulations, there are a total of 4096 data bits which are coded, interleaved and then modulated. The modulated symbols are distributed to the transmit antennas in a sequential order as given in Fig. 5.1.

For the LLR exchange between the LMMSE equalizer and the APP decoder, we use the Wang-Poor approach through a straightforward extension of Section 2.2.3 to MIMO systems. In addition, we apply some scaling operations to the extrinsic LLR values at the output of the LMMSE equalizer and the APP decoder so as to prevent overconfident messages. Once more, we use a scaling factor ρ which divides the LLR values at the output of the APP decoder and we operate the proposed factor graph based LMMSE equalizer under the assumption that the noise variables have variance values γN_0 larger than the actual value $(\gamma > 1)$. The judiciously determined values of

ρ and γ are indicated below the related figure. By this way, we decrease the extrinsic LLR values, or the confidence of messages, at the output of both our equalizer and the APP decoder at each turbo iteration. In addition, we did not try to optimize the scaling factors for each SNR value due to our practicality concerns contrary to [19].

For all the configurations below, we also provide the matched filter bound (MFB) performances as a benchmark to make a comparison. The MFB performances are obtained under the assumption that the symbols which cause interference to the interested symbol due to multi-path and multi-antenna effects are perfectly known by the receiver for each interested symbol [4]. Hence, it is practically impossible to reach MFB performance for any receiver structure. We take MFB performance as a genie-aided lower bound for the proposed scheme.

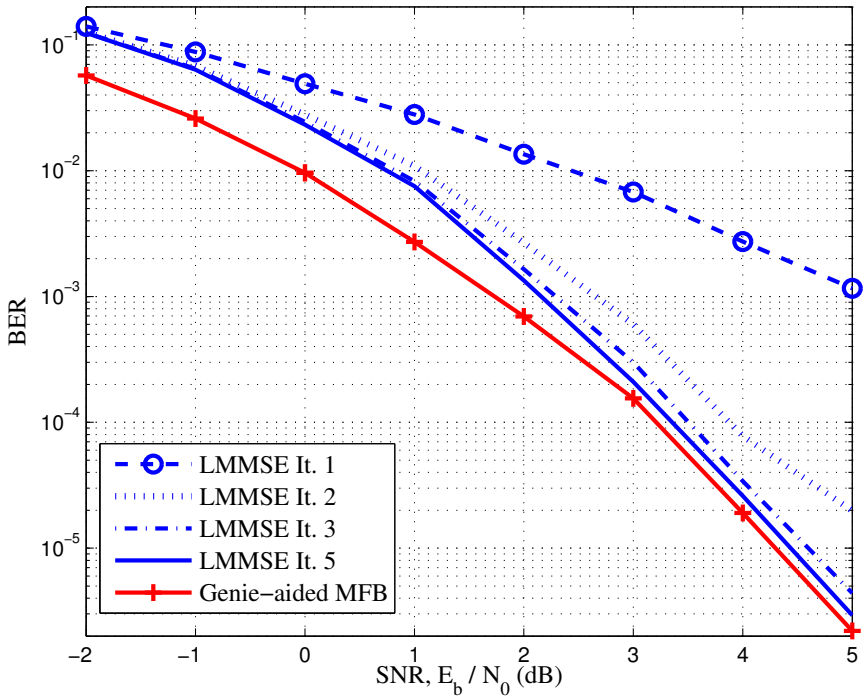

Figure 5.3: BER Performance of the Factor Graph Based LMMSE Equalizer (2×2 MIMO with $L = 5$ for BPSK Signaling, $\rho = 1.5$, $\gamma = 2$)

The BER performance of the proposed factor graph based LMMSE equalizer is given in Fig. 5.3 for BPSK signalling with $N_t = N_r = 2$ under a 5-tap channel. This is the same configuration as the one in [12] except the interleaver type which is S-

random in [12]. The proposed method has nearly identical performance with the one in [12] for low SNR values as expected since both algorithms implement time domain LMMSE filtering operation. Moreover, the error floor observed in high SNR regions in [12] which may be caused by its extrinsic LLR exchange algorithm does not occur here. Also, the performance of the proposed method is very close to the MFB below the BER value of 10^{-3} without any diversity loss or error floor. In addition, it can be seen that there is no significant improvement after three turbo iterations which means only three iterations are sufficient for this configuration.

The simulation scheme in [43] which presented the performance results of both time and frequency domain LMMSE equalization for Gray encoded QPSK signaling is additionally compared with our method. We observe the performance of the proposed LMMSE equalizer for both of the extrinsic LLR computation methods which are explained as the exact Wang Poor (WP) based algorithm in (2.37) and the approximated version in (2.39). As seen from Fig. 5.4, for which the exact WP based algorithm is operated, the performance of the proposed LMMSE equalizer is very close to the MFB performance so that the difference between them is less than 0.5 dB below BER value of 10^{-3} in only 4 turbo iterations. Moreover, it is observed that there is no necessity of any scaling operation for LLR values. This makes the proposed structure more practical for real time applications. In addition, the performance result of our proposed algorithm and the curves presented in [43] for time domain LMMSE equalization performance are identical as expected. Frequency domain LMMSE equalization in [43] has a small SNR loss as compared to the time domain versions due to overhead caused by the addition of a cyclic prefix.

In Fig. 5.5, the same setting as in the Fig. 5.4 is used with the approximated version of the WP based LLR computation algorithm in (2.39) under 5 turbo iterations. The judiciously chosen scaling factors, which are indicated in Fig. 5.5, are observed to improve the performance. As shown by Fig. 5.4-5.5, performance results are close to each other. However, exact WP based algorithm provides slightly better convergence to MFB than approximated version using one less turbo iterations.

Also, we present here the performance of a more challenging scenario with higher order constellations which was not presented in the studies including Gaussian ap-

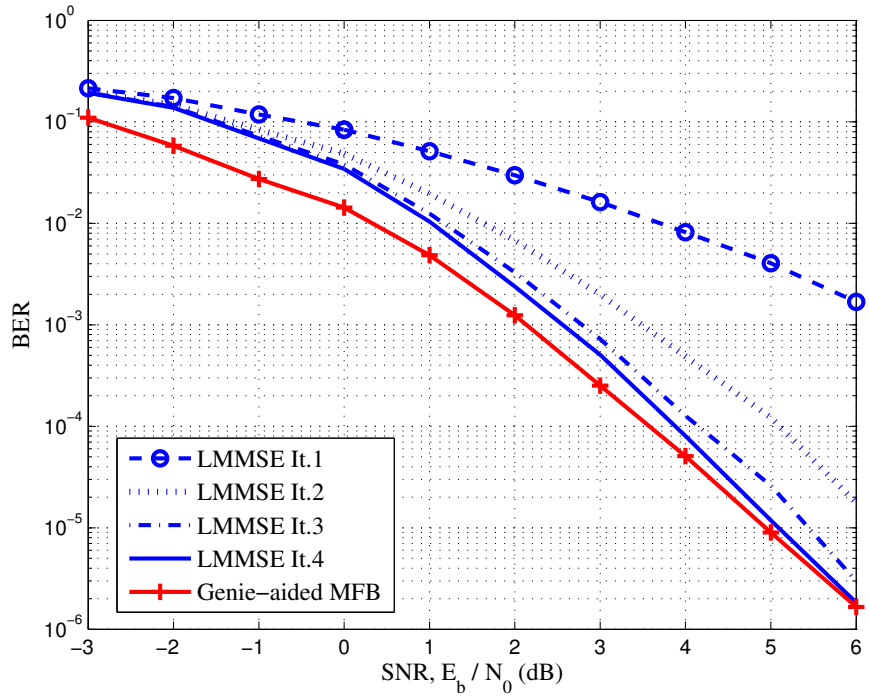

Figure 5.4: BER Performance of the Factor Graph Based LMMSE Equalizer with Exact WP Based LLR Computation (2×2 MIMO with $L = 4$ for QPSK Signaling, $\rho = 1,\ \gamma = 1$)

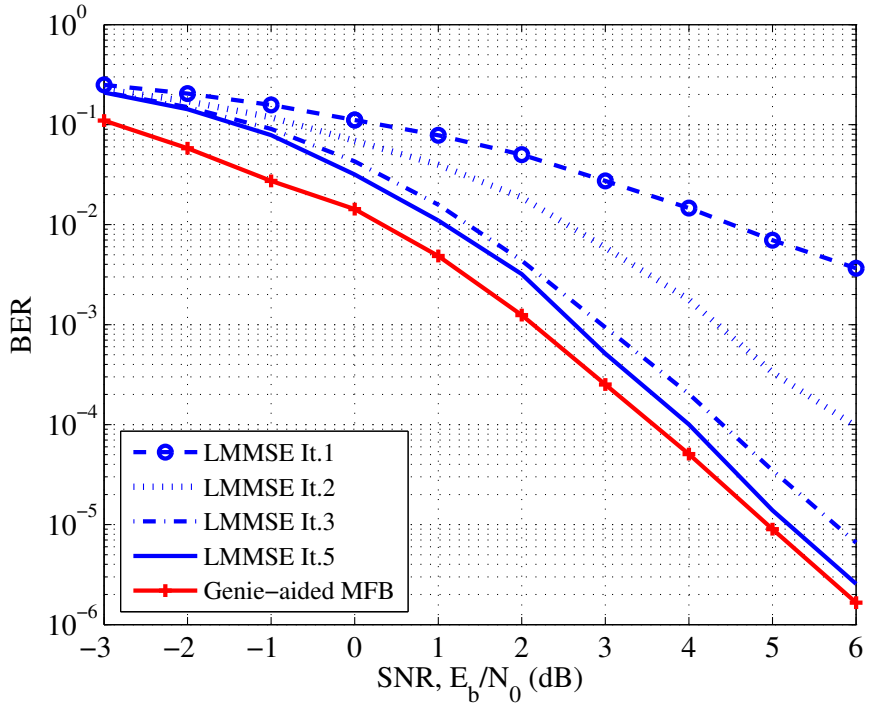

Figure 5.5: BER Performance of the Factor Graph Based LMMSE Equalizer with Approximated WP Based LLR Computation (2×2 MIMO with $L = 4$ for QPSK Signaling, $\rho = 1.25,\ \gamma = 3$)

proximation over a factor graph in the literature so far. For Gray encoded 16-QAM signaling, we observe the performance of the proposed LMMSE equalizer for both of the extrinsic LLR computation methods which are explained as the exact Wang Poor (WP) based algorithm in (2.37) and the approximated version in (2.39). Here, a 4-tap Rayleigh ISI channel is used with $N_t = N_r = 2$. Fig. 5.6 depicts simulation results of the LMMSE equalizer with the exact WP based LLR computation algorithm. It can be seen from Fig. 5.6 that the proposed method has a performance which is less than 1 dB away from the MFB performance below the BER value of 10^{-4} for 7 turbo iterations. Moreover, it is observed that there is no necessity of any scaling operation for LLR values. The increased constellation size leads to a higher number of turbo iterations for good performance, but turbo iteration number is not a direct multiplier of computational complexity since all packets do not require 7 iterations. Moreover, the constellation size does not affect the modulation complexity per turbo iteration. Hence, our method is a practical choice as a receiver structure with its solid performance so as to achieve higher data rates.

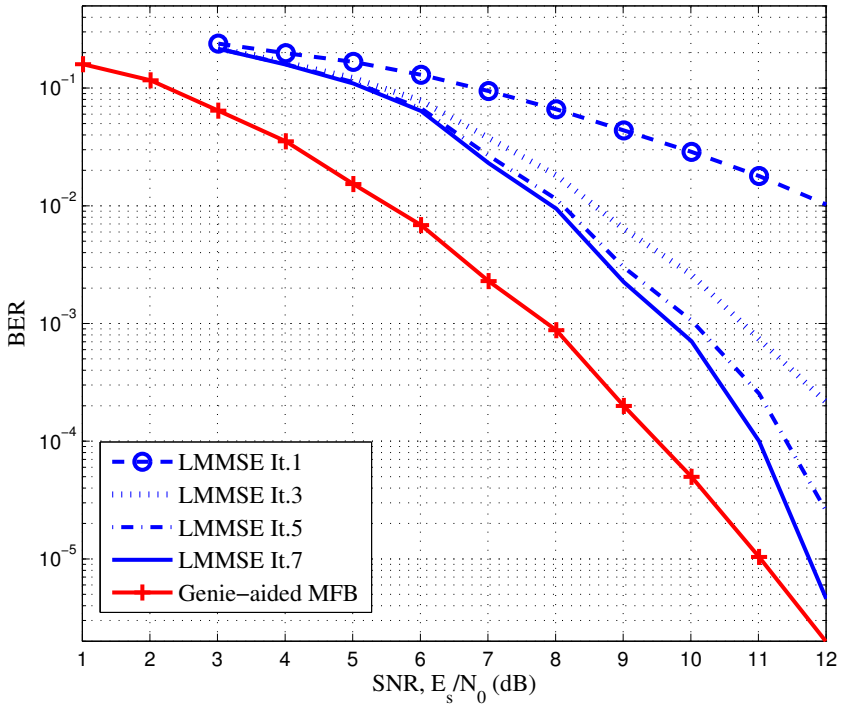

Figure 5.6: BER Performance of the Factor Graph Based LMMSE Equalizer with Exact WP Based LLR Computation(2×2 MIMO with $L = 4$ for 16-QAM Signaling, $\rho = 1,\ \gamma = 1$)

In Fig. 5.7, the same setting as in the Fig. 5.6 is used with the approximated version of the WP based LLR computation algorithm in (2.39) under 10 turbo iterations. The judiciously chosen scaling factors, which are indicated in Fig. 5.7, are observed to improve the performance. As shown by Fig. 5.6-5.7, performance results are close to each other. However, exact WP based algorithm provides slightly better convergence to MFB than approximated version using less turbo iterations.

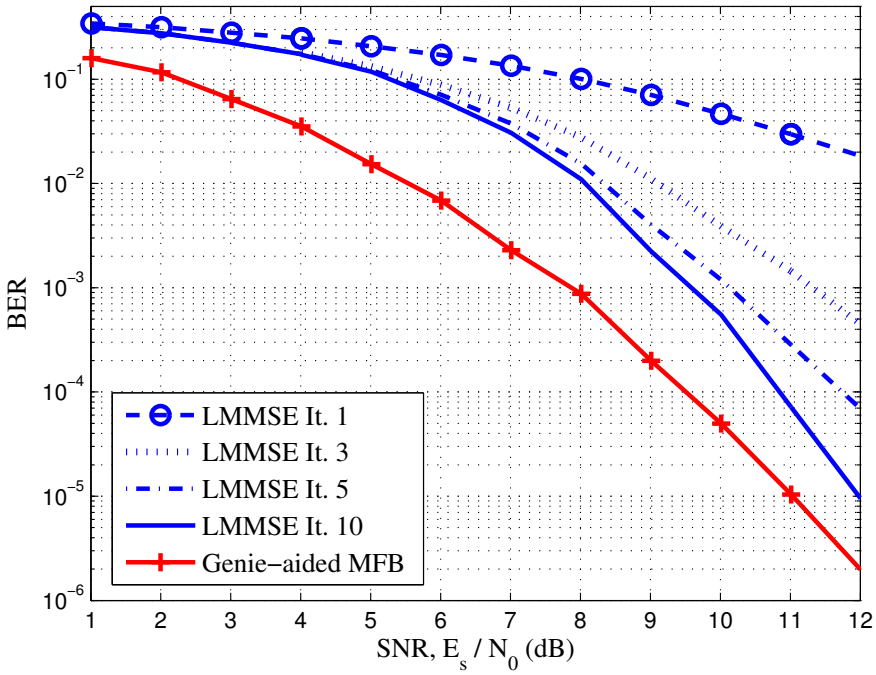

Figure 5.7: BER Performance of the Factor Graph Based LMMSE Equalizer with Approximated WP Based LLR Computation (2×2 MIMO with $L = 4$ for 16-QAM Signaling, $\rho = 1,\ \gamma = 2$)

CHAPTER 6

CONCLUSION

In this study, we have focused on a reduced complexity graph based LMMSE filtering technique which can be used as a practical equalizer to remove the ISI effect in wireless channels. Based on a previously proposed graph structure in the literature, we make some improvements for wireless communication problems. First, we develop an efficient way of computing extrinsic LLR values after LMMSE equalization for M-QAM constellations. We have shown the mathematical relation between the output of the LMMSE equalizer and the popular Wang-Poor method's parameters in a suitable fashion for factor graphs. It provides easy implementation of LMMSE filtering that can be used with high order modulation alphabets on which LMMSE filtering is more advantageous owing to the Gaussian assumption.

In addition, we propose a reduced complexity factor graph-based LMMSE filtering method for non-white noise processes which are encountered in some communication and signal processing problems such as FTN signaling, clutter suppression in radar systems and speech enhancement. Our method in which the statistics of the colored noise are taken into account seems to be an attractive solution to implement the LMMSE filtering operation owing to its computational complexity linearly increasing with block length of the input signal. The equivalence to LMMSE filtering is shown through extensive simulations for Gaussian AR noise processes. Moreover, the generalization to other stationary processes with known (or estimated) autocorrelation function through an approximation to a proper order AR process is also considered in our work.

To provide an application for the mentioned approximation method, we analyze FTN

signaling as a recently popular subject, which inherently involves the effects of both ISI and the non-white noise. We propose to use our reduced complexity graph-based LMMSE equalizer, which incorporates the statistics of the noise signal into the factor graph by modelling it as an AR process. For configurations with different noise statistics, we show that the proposed low complexity receiver structure performs close to the optimal decoder operating in ISI-free ideal scenario without FTN signaling through simulations. However, we have also observed that there is a tradeoff between the performance gain and computational complexity caused by the increasing approximation order used in the AR process approximation. Therefore, our method comes forefront particularly for applications involving high noise correlations in which taking the noise statistics into consideration even with small approximation order values provides significant performance gain.

In the last part, we enlarge the factor graph structure for the LMMSE equalization to frequency selective MIMO channels. The proposed graph has the advantage of low complexity as compared to the conventional block LMMSE filtering operation and the other graph based LMMSE filtering approaches in the literature. In addition, the straightforward generalization of our proposed extrinsic bit LLR computation method for LLMSE equalizer to the MIMO ISI scenario is used. To sum up, we proposed a low complexity, practical LMMSE equalizer for iterative decoding of MIMO ISI channels with a good performance as confirmed by our simulation results. Our method here is attractive for higher constellation sizes since its computational complexity is not affected by the dimension of the signalling space owing to the Gaussian assumption used in the factor graph.

For future work, it will be interesting to observe or analyse the limits of the LMMSE equalizer in FTN signalling since we cannot reach very high data rates due to degradation in BER performance of LMMSE equalizer. In addition, the performance of the proposed LMMSE equalizer here, which incorporates the non-white statistics of noise process, can be investigated in other high noise correlation applications such as channel shortening or multi-user communication as compared to the other techniques in the literature. In order to reduce the computational complexity for MIMO systems, the proposed graph structure can be modified in a loopy manner, i.e., it is not cycle free any more. Moreover, if the graph structure for MIMO systems can be adapted

for colored noise processes in a similar way to SISO systems explained here, FTN will also be implemented in MIMO systems using the LMMSE equalizer through this newly modified graph structure.

REFERENCES

[1] J. Anderson, F. Rusek, and V. Owall. Faster-than-Nyquist signaling. *Proceedings of the IEEE*, 101(8):1817–1830, 2013.

[2] K. Baddour and N. Beaulieu. Autoregressive modeling for fading channel simulation. *Wireless Communications, IEEE Transactions on*, 4(4):1650–1662, July 2005.

[3] L. Bahl, J. Cocke, F. Jelinek, and J. Raviv. Optimal decoding of linear codes for minimizing symbol error rate (corresp.). *Information Theory, IEEE Transactions on*, 20(2):284–287, March 1974.

[4] J. R. Barry, E. A. Lee, and D. G. Messerschmitt. *Digital Communications*. Springer, 2004.

[5] J. Bergin, P. Techau, J. Don Carlos, and J. Guerci. Radar waveform optimization for colored noise mitigation. In *Radar Conference, 2005 IEEE International*, pages 149–154, 2005.

[6] D. Bertsekas and J. Tsitsiklis. *Introduction to Probability*. Athena Scientific books. Athena Scientific, 2002.

[7] U. N. Bhat and G. K. Miller. *Elements of applied stochastic processes*. J. Wiley, 1972.

[8] G. Colavolpe, G. Ferrari, and R. Raheli. Reduced-state BCJR-type algorithms. *Selected Areas in Communications, IEEE Journal on*, 19(5):848–859, 2001.

[9] G. Colavolpe, D. Fertonani, and A. Piemontese. SISO detection over linear channels with linear complexity in the number of interferers. *Selected Topics in Signal Processing, IEEE Journal of*, 5(8):1475–1485, December 2011.

[10] G. Colavolpe and G. Germi. On the application of factor graphs and the sum-product algorithm to ISI channels. *Communications, IEEE Transactions on*, 53(5):818–825, May 2005.

[11] R. Drost and A. Singer. Factor-graph algorithms for equalization. *Signal Processing, IEEE Transactions on*, 55(5):2052–2065, May 2007.

[12] B. Etzlinger, W. Haselmayr, and A. Springer. Equalization algorithms for MIMO communication systems based on factor graphs. In *Communications (ICC), 2011 IEEE International Conference on*, pages 1–5, June 2011.

[13] D. Falconer, S. Ariyavisitakul, A. Benyamin-Seeyar, and B. Eidson. Frequency domain equalization for single-carrier broadband wireless systems. *Communications Magazine, IEEE*, 40(4):58–66, April 2002.

[14] D. Fertonani, A. Barbieri, and G. Colavolpe. Reduced-complexity BCJR algorithm for turbo equalization. *Communications, IEEE Transactions on*, 55(12):2279–2287, December 2007.

[15] J. Gibson, B. Koo, and S. Gray. Filtering of colored noise for speech enhancement and coding. *Signal Processing, IEEE Transactions on*, 39(8):1732–1742, 1991.

[16] Q. Guo and D. Huang. A concise representation for the soft-in soft-out LMMSE detector. *IEEE Commun. Lett.*, 15(5):566 –568, May 2011.

[17] Q. Guo and L. Ping. LMMSE turbo equalization based on factor graphs. *Selected Areas in Communications, IEEE Journal on*, 26(2):311–319, 2008.

[18] G. Guvensen and A. Yilmaz. A general framework for optimum iterative blockwise equalization of single carrier MIMO systems and asymptotic performance analysis. *Communications, IEEE Transactions on*, 61(2):609–619, February 2013.

[19] W. Haselmayr, B. Etzlinger, and A. Springer. Equalization of MIMO-ISI channels based on Gaussian message passing in factor graphs. In *Turbo Codes and Iterative Information Processing (ISTC), 2012 7th International Symposium on*, pages 76–80, August 2012.

[20] W. Hassasneh, A. Jamoos, E. Grivel, and H. Nour. Estimation of mc-ds-cdma fading channels based on kalman filtering with high order autoregressive models. In *Mobile Computing and Wireless Communication International Conference, 2006. MCWC 2006. Proceedings of the First*, pages 145–149, September 2006.

[21] C. R. Johnson. *Matrix theory and applications*, volume 40. American Mathematical Soc., 1990.

[22] S. M. Kay. *Fundamentals of Statistical Signal Processing: Estimation Theory*. Prentice-Hall, Inc., 1993.

[23] M. Kaynak, T. Duman, and E. Kurtas. Belief propagation over SISO/MIMO frequency selective fading channels. *Wireless Communications, IEEE Transactions on*, 6(6):2001–2005, June 2007.

[24] S. Korl. *A Factor Graph Approach to Signal Modelling, System Identification and Filtering*. Ph.d. dissertation, Swiss Federal Institude of Technology, Zürich, Sweeden, 2005.

[25] L. Liu, W. K. Leung, and L. Ping. Simple iterative chip-by-chip multiuser detection for CDMA systems. In *Vehicular Technology Conference, 2003. VTC 2003-Spring. The 57th IEEE Semiannual*, volume 3, pages 2157–2161 vol.3, April 2003.

[26] H.-A. Loeliger. Least squares and Kalman filtering on Forney graphs. In R. Blahut and R. Koetter, editors, *Codes, Graphs, and Systems*, volume 670 of *The Kluwer International Series in Engineering and Computer Science*, pages 113–135. Springer US, 2002.

[27] H.-A. Loeliger. An introduction to factor graphs. *Signal Processing Magazine, IEEE*, 21(1):28–41, January 2004.

[28] H.-A. Loeliger, J. Dauwels, J. Hu, S. Korl, L. Ping, and F. Kschischang. The factor graph approach to model-based signal processing. *Proceedings of the IEEE*, 95(6):1295–1322, 2007.

[29] H.-A. Loeliger, J. Hu, S. Korl, Q. Guo, and L. Ping. Gaussian Message Passing on linear models: An update. In *Turbo Codes Related Topics; 6th International ITG-Conference on Source and Channel Coding (TURBOCODING), 2006 4th International Symposium on*, pages 1–7, 2006.

[30] J. Mazo. Faster-than-nyquist signaling. *Bell Syst. Tech. J*, 54(8):1451–1462, 1975.

[31] F. Pancaldi, G. Vitetta, R. Kalbasi, N. Al-Dhahir, M. Uysal, and H. Mheidat. Single-carrier frequency domain equalization. *Signal Processing Magazine, IEEE*, 25(5):37–56, September 2008.

[32] A. Prlja and J. Anderson. Reduced-complexity receivers for strongly narrowband intersymbol interference introduced by faster-than-Nyquist signaling. *Communications, IEEE Transactions on*, 60(9):2591–2601, September 2012.

[33] J. Proakis and M. Salehi. *Digital communications*. McGraw-Hill Education, fifth edition, 2007.

[34] A. Radosevic, D. Fertonani, T. Duman, J. Proakis, and M. Stojanovic. Bounds on the information rate for sparse channels with long memory and i.u.d. inputs. *Communications, IEEE Transactions on*, 59(12):3343–3352, 2011.

[35] S. Roy and T. Duman. Soft input soft output Kalman equalizer for MIMO frequency selective fading channels. *Wireless Communications, IEEE Transactions on*, 6(2):506–514, February 2007.

[36] F. Rusek. *Partial Response and Faster-than-Nyquist Signaling*. Ph.d. dissertation, Dept. of Electrical and Information Technology, Lund University, Lund, Sweeden, 2007.

[37] F. Rusek and J. B. Anderson. On information rates for faster than Nyquist signaling. *IEEE Trans. Commun.*, 53(5):818 – 825, May 2006.

[38] P. Sen, T. Aktas, and A. Yilmaz. A low-complexity graph-based LMMSE receiver designed for colored noise induced by FTN-signaling. In *Wireless Communications and Networking Conference (WCNC), 2014 IEEE*, April 2014.

[39] S. Sugiura. Frequency-domain equalization of faster-than-Nyquist signaling, 2013.

[40] M. Tüchler, R. Koetter, and A. Singer. Turbo equalization: principles and new results. *Communications, IEEE Transactions on*, 50(5):754–767, 2002.

[41] M. Tüchler, A. Singer, and R. Koetter. Minimum mean squared error equalization using a priori information. *Signal Processing, IEEE Transactions on*, 50(3):673–683, March 2002.

[42] X. Wang and H. Poor. Iterative (turbo) soft interference cancellation and decoding for coded CDMA. *Communications, IEEE Transactions on*, 47(7):1046–1061, 1999.

[43] X. Yuan, Q. Guo, and L. Ping. Low-complexity iterative detection in multi-user MIMO ISI channels. *Signal Processing Letters, IEEE*, 15:25–28, 2008.